



PB94-156908

Publication No. FHWA-RD-92-090
January 1994

Impact Characteristics of Glass Fiber-Reinforced Composite Materials for use in Roadside Safety Barriers



U.S. Department of Transportation
Federal Highway Administration

Research and Development
Turner-Fairbank Highway Research Center
6300 Georgetown Pike
McLean, Virginia 22101-2296

REPRODUCED BY:
U.S. Department of Commerce
National Technical Information Service
Springfield, Virginia 22161

FOREWORD

This report presents the results from a preliminary investigation on the suitability of glass-fiber reinforced composite materials for roadside safety hardware, specifically, barrier structures. The results from two series of laboratory drop-weight impact tests on these materials are presented here. It is a comprehensive collection of instrumented impact test data plots and methods for data interpretation. Also, design considerations and possibilities for future investigations are given. This report will be of interest to structural engineers concerned with the dynamic behavior of composites and will be used as a reference to guide further FHWA studies on composites for roadside safety structures.



Lyle Saxton
Director, Office of Safety and Traffic
Operations Research and Development


NOTICE

This document is disseminated under the sponsorship of the Department of Transportation in the interest of information exchange. The United States Government assumes no liability for its contents or use thereof.

The contents of this report reflect the views of the author, who is responsible for the facts and accuracy of the data presented herein. The contents do not necessarily reflect the official policy of the Department of Transportation.

This report does not constitute a standard, specification, or regulation.

The United States Government does not endorse products or manufacturers. Trade or manufacturers' names appear herein only because they are considered essential to the object of this document.

1. Report No. FHWA-RD-93-090	2.  PB94-156908	3. Recipient's Catalog No.	
4. Title and Subtitle IMPACT CHARACTERISTICS OF GLASS FIBER-REINFORCED COMPOSITE MATERIALS FOR USE IN ROADSIDE SAFETY BARRIERS		5. Report Date January 1994	6. Performing Organization Code
7. Author(s) Alrik L. Svenson		8. Performing Organization Report No.	
9. Performing Organization Name and Address Turner-Fairbank Highway Research Center 6300 Georgetown Pike McLean, Virginia 22101-2296		10. Work Unit No. (TRAIS) 3A5D-0262	11. Contract or Grant No. NHI GRF Project #91-4
12. Sponsoring Agency Name and Address Office of Safety and Traffic Operations R&D Federal Highway Administration 6300 Georgetown Pike McLean, Virginia 22101-2296		13. Type of Report and Period Covered Final Report July 1991 - December 1992	
15. Supplementary Notes Author's M.C.E. Thesis, The Catholic University of America, Washington, DC		14. Sponsoring Agency Code	
16. Abstract The Federal Highway Administration (FHWA) is interested in the development of barriers composed of composite materials. Barriers, as well as other roadside safety appurtenances are structures subjected to dynamic loading by errant vehicles. This investigation focuses on the understanding of the impact behavior of fiber-reinforced composites when subjected to low-velocity impacts, such as an automobile collision into a fixed roadside object. This study attempts to characterize the relative impact performance of several different fiber architecture types in glass fiber-reinforced composites. This dynamic characterization of materials compared test specimens cut from standard, commercially available glass fiber-reinforced pultruded composite shapes with laboratory-fabricated composites of four different fiber geometries. Composite plates were fabricated by a hand lay-up vacuum bag process and were then cut into impact test specimens approximately 178 mm long by 25 mm wide (7.0 in long by 1.0 in wide). These test specimens were used to evaluate the impact characteristics of the various types of materials. This report discusses the drop weight testing procedures, important data analysis parameters, and material fabrication methods used in this study. The results of impact tests on both pultruded and laboratory-fabricated composite samples are presented and compared. Also, design considerations and possibilities for further investigations are recommended.			
17. Key Words Instrumented impact testing, composite materials, glass fiber-reinforced plastics, roadside safety structures.		18. Distribution Statement No restrictions. This document is available to the public through the National Technical Information Service, Springfield, Virginia 22161.	
19. Security Classif. (of this report) Unclassified	20. Security Classif. (of this page) Unclassified	21. No of Pages 72	22. Price

PREFACE

The Federal Highway Administration (FHWA) is interested in the development of barriers composed of fiber-reinforced composite materials. Barriers, as well as other roadside safety appurtenances, are structures subjected to dynamic loading by errant vehicles. This investigation focuses on the understanding of the impact behavior of fiber-reinforced composites when subjected to low-velocity impacts, such as an automobile collision into a fixed roadside object. This study attempts to characterize the relative impact performance of several different fiber architecture types in glass fiber-reinforced composites.

This dynamic characterization of materials compared test specimens cut from standard, commercially available glass fiber-reinforced pultruded composite shapes with laboratory-fabricated composites of four different fiber geometries. The laboratory-fabricated material consisted of the following fiber types: unidirectional fibers [0 rad (0°) and 1.57 rad (90°) axes], a 0 rad (0°) to 1.57 rad (90°) woven roving, a ± 0.785 rad (45°) stitched roving, and a chopped random-strand mat. In addition, both polyester and vinyl ester resins were compared. These resins had tensile elongations ranging from 2 percent to 20 percent. Composite plates were fabricated by a hand lay-up vacuum bag process and were then cut into impact test specimens approximately 178 mm long by 25 mm wide (7.0 in long by 1.0 in wide). These test specimens were used to evaluate impact characteristics of the various combinations of materials.

This thesis discusses the drop weight impact testing procedures, important data analysis parameters, and material fabrication methods used in this study. The results of impact tests on both pultruded and laboratory-fabricated composite samples are presented and compared. Also, design considerations and possibilities for further investigations are recommended.

SI* (MODERN METRIC) CONVERSION FACTORS

APPROXIMATE CONVERSIONS TO SI UNITS

APPROXIMATE CONVERSIONS FROM SI UNITS

Symbol	When You Know	Multiply By	To Find	Symbol	Symbol	When You Know	Multiply By	To Find	Symbol
LENGTH					LENGTH				
in	inches	25.4	millimeters	mm	mm	millimeters	0.039	inches	in
ft	feet	0.305	meters	m	m	meters	3.28	feet	ft
yd	yards	0.914	meters	m	m	meters	1.09	yards	yd
mi	miles	1.61	kilometers	km	km	kilometers	0.621	miles	mi
AREA					AREA				
in ²	square inches	645.2	square millimeters	mm ²	mm ²	square millimeters	0.0016	square inches	in ²
ft ²	square feet	0.093	square meters	m ²	m ²	square meters	10.764	square feet	ft ²
yd ²	square yards	0.836	square meters	m ²	m ²	square meters	1.195	square yards	ac
ac	acres	0.405	hectares	ha	ha	hectares	2.47	acres	mi ²
mi ²	square miles	2.59	square kilometers	km ²	km ²	square kilometers	0.386	square miles	
VOLUME					VOLUME				
fl oz	fluid ounces	29.57	milliliters	ml	ml	milliliters	0.034	fluid ounces	fl oz
gal	gallons	3.785	liters	l	l	liters	0.264	gallons	gal
ft ³	cubic feet	0.028	cubic meters	m ³	m ³	cubic meters	35.71	cubic feet	ft ³
yd ³	cubic yards	0.765	cubic meters	m ³	m ³	cubic meters	1.307	cubic yards	yd ³
MASS					MASS				
oz	ounces	28.35	grams	g	g	grams	0.035	ounces	oz
lb	pounds	0.454	kilograms	kg	kg	kilograms	2.202	pounds	lb
T	short tons (2000 lb)	0.907	megagrams	Mg	Mg	megagrams	1.103	short tons (2000 lb)	T
TEMPERATURE (exact)					TEMPERATURE (exact)				
°F	Fahrenheit temperature	5(F-32)/9 or (F-32)/1.8	Celcius temperature	°C	°C	Celcius temperature	1.8C + 32	Fahrenheit temperature	°F
ILLUMINATION					ILLUMINATION				
fc	foot-candles	10.76	lux	l	lx	lux	0.0929	foot-candles	fc
fl	foot-Lamberts	3.426	candela/m ²	cd/m ²	cd/m ²	candela/m ²	0.2919	foot-Lamberts	fl
FORCE and PRESSURE or STRESS					FORCE and PRESSURE or STRESS				
lbf	poundforce	4.45	newtons	N	N	newtons	0.225	poundforce	lbf
psi	poundforce per square inch	6.89	kilopascals	kPa	kPa	kilopascals	0.145	poundforce per square inch	psi

* SI is the symbol for the International System of Units. Appropriate rounding should be made to comply with Section 4 of ASTM E380.

(Revised August 1992)

TABLE OF CONTENTS

Chapter

1. INTRODUCTION	1
2. IMPACT TESTING PROCEDURES	3
Testing Apparatus	3
Test Methods	3
Analysis of Impact Test Data	5
3. IMPACT TESTS ON PULTRUDED COMPOSITE MATERIALS	7
Test Specimens	7
Test Results	7
4. LABORATORY FABRICATION OF COMPOSITE MATERIALS	35
Fabrication Procedure	35
Test Specimens	35
5. IMPACT TESTS ON LABORATORY-FABRICATED MATERIAL	37
Test Results	37
Comparison with Pultruded Material	37
6. DESIGN CONSIDERATIONS	61
Data Analysis, Testing, and Design	61
Future Investigations	61
7. CONCLUSIONS	63
REFERENCES	65

LIST OF FIGURES

Figure No.

1. Experimental setup	4
2. Typical velocity versus time plot	4
3. Important data analysis points	6
4. Load versus time (LV2)	8
5. Load versus time (LV3)	9
6. Load versus time (LV4)	9
7. Load versus time (LP3)	10
8. Load versus time (TP3)	10
9. Load versus time (TV3)	11
10. Load versus time (TV4)	11
11. Energy versus time (LV2)	12
12. Energy versus time (LV3)	12
13. Energy versus time (LV4)	13
14. Energy versus time (LP3)	13
15. Energy versus time (TP3)	14
16. Energy versus time (TV3)	14
17. Energy versus time (TV4)	15
18. Average load versus time (LV2)	15
19. Average load versus time (LV3)	16
20. Average load versus time (LV4)	16
21. Average load versus time (LP3)	17
22. Average load versus time (TP3)	17
23. Average load versus time (TV3)	18
24. Average load versus time (TV4)	18
25. Average energy versus time (LV2)	19
26. Average energy versus time (LV3)	19
27. Average energy versus time (LV4)	20
28. Average energy versus time (LP3)	20
29. Average energy versus time (TP3)	21
30. Average energy versus time (TV3)	21
31. Average energy versus time (TV4)	22
32. Standard deviation (LV2)	22
33. Standard deviation (LV3)	23
34. Standard deviation (LV4)	23
35. Standard deviation (LP3)	24
36. Standard deviation (TP3)	24
37. Standard deviation (TV3)	25
38. Standard deviation (TV4)	25
39. Normalized load (by area) - pultruded	26
40. Normalized energy (by area) - pultruded	26
41. Normalized load (by all geometry) - pultruded	28
42. Normalized energy (by all geometry) - pultruded	28
43. Impact sequence (LV3) at time 0, 4, 6, 8, and 16 ms	30
44. Impact sequence (LV4) at time 0, 3, 7, 9, and 14 ms	31
45. Impact sequence (LP3) at time 0, 6, 8, 12, and 17 ms	32
46. Laboratory fabrication	36
47. Load versus time (CE)	38
48. Load versus time (CA)	38
49. Load versus time (CH)	39
50. Load versus time (CV)	39
51. Load versus time (LE)	40

LIST OF FIGURES (Continued)

Figure No.

52. Load versus time (LA)	40
53. Load versus time (LH)	41
54. Load versus time (LV)	41
55. Energy versus time (CE)	42
56. Energy versus time (CA)	42
57. Energy versus time (CH)	43
58. Energy versus time (CV)	43
59. Energy versus time (LE)	44
60. Energy versus time (LA)	44
61. Energy versus time (LH)	45
62. Energy versus time (LV)	45
63. Average load versus time (CE)	46
64. Average load versus time (CA)	46
65. Average load versus time (CH)	47
66. Average load versus time (CV)	47
67. Average load versus time (LE)	48
68. Average load versus time (LA)	48
69. Average load versus time (LH)	49
70. Average load versus time (LV)	49
71. Average energy versus time (CE)	50
72. Average energy versus time (CA)	50
73. Average energy versus time (CH)	51
74. Average energy versus time (CV)	51
75. Average energy versus time (LE)	52
76. Average energy versus time (LA)	52
77. Average energy versus time (LH)	53
78. Average energy versus time (LV)	53
79. Standard deviation (CE)	54
80. Standard deviation (CA)	54
81. Standard deviation (CH)	55
82. Standard deviation (CV)	55
83. Standard deviation (LE)	56
84. Standard deviation (LA)	56
85. Standard deviation (LH)	57
86. Standard deviation (LV)	57
87. Normalized load - laboratory fabricated	58
88. Normalized energy - laboratory fabricated	58

LIST OF TABLES

Table No.

1. Test specimen specifications	8
2. Average values	29
3. Average thickness - laboratory-fabricated material	36
4. Average values - laboratory-fabricated material	59

CHAPTER 1. INTRODUCTION

The Federal Highway Administration (FHWA) is currently studying innovative structural applications of fiber-reinforced composite materials. Some potential applications are roadside safety structures. These include: barriers such as guardrails and cable-type barriers, signs, energy-absorbing crash cushions, and luminaire supports. Roadside safety structures, in general, must perform acceptably to meet current crash-test standards while at the same time, be "forgiving" to vehicle occupants.⁽¹⁾ This thesis discusses the feasibility of using composite materials based on the results of small-scale drop-weight impact testing. In particular, the suitability of these materials for barrier structures is investigated.

The purpose of a roadside barrier is to minimize the hazards to vehicle occupants associated with an errant vehicle leaving the roadway.⁽²⁾ Two goals are to maintain the structural integrity of the barrier (i.e., to prevent the impacting vehicle from penetrating through) and to maximize the energy absorbed by the barrier. This energy absorption, in effect, reduces the impacting vehicle's velocity by converting the kinetic energy of the vehicle into a deformation of the barrier. In addition, for an oblique impact, additional kinetic energy is dissipated through friction losses as the vehicle scrapes along the length of the barrier without penetrating. This scraping action also contributes to a reduction of the vehicle velocity while redirecting the vehicle nearly parallel to the roadway.⁽³⁾ The barrier must also be designed to provide a net resistance force at or near the vehicle's center of gravity to reduce the possibility of overturning the vehicle following the collision. Thus, a barrier must not only be able to contain and redirect the vehicle, it must be able to reduce the risk of various hazards associated with the collision event.⁽¹⁾

This study focuses on understanding the impact characteristics of glass fiber-reinforced plastics when subjected to dynamic loadings. Glass fiber reinforcement is considered because glass reinforcement has one of the highest energy absorption rates and one of the lowest costs when compared with other composite reinforcement materials.⁽⁴⁾ The dynamic loading of test specimens (conducted in a laboratory environment), is similar to vehicle impacts into fixed roadside objects, such as a barrier. All of the impact-testing research has been conducted at the FHWA Turner-Fairbank Highway Research Center (TFHRC) located in McLean, Virginia. A vertical drop-weight test machine instrumented with an accelerometer attached to the striker has been used to obtain the test results reported here.



CHAPTER 2. IMPACT TESTING PROCEDURES

Testing Apparatus

An MTS Vertical Drop-Weight Test Machine, model 850.02A-01 was used to conduct the impact tests. The drop weight and striker together had a mass of 82 kg (181 lb). A drop height of 0.457 m (1.5 ft) was maintained for all tests. This produced an initial impact energy of 380 J (271.5 ft-lb). An accelerometer affixed to the drop weight yielded the complete acceleration versus time history of the impact event. The output from the accelerometer was collected by a computer and data acquisition system at a sampling rate of 37,878.788 samples per second. The data acquisition system was triggered by a switch as the falling weight passed. The switch was tripped immediately before impact with the specimen. Each specimen was tested simply supported on a 152-mm (6-in) span. The cylindrical striker head was 63.5 mm long by 12.7 mm wide (2.5 in long by 0.5 in wide). The specimens were struck at the center of the span as shown in figure 1. All testing was performed in laboratory conditions at room temperature. After data from a test was obtained, it was imported into a spreadsheet for load, energy, and velocity calculations.⁽³⁾ Also, many of the tests were filmed by a high-speed camera at a rate of 1,000 frames per second. This provided useful information during the analysis of data.

Test Methods

Immediately after release of the drop weight, until the moment of impact with the specimen, the striker's acceleration is constant and equal to the gravitational acceleration (losses due to friction and air resistance are neglected). Therefore, the velocity of the striker increases at a linear rate during free fall. At impact, the striker's velocity can be expressed by the relationship,

$$v_0 = gt_0 = [2gh_0]^{\frac{1}{2}} \quad (1)$$

where v_0 is the striker velocity at impact, g is the acceleration of gravity, 9.8 m/s^2 (32.2 ft/s^2), t_0 is the time between release and impact, and h_0 is the drop height.⁽³⁾

The instantaneous velocity of the striker becomes non-linear during and after impact and is reduced as a result of the flexural resistance of the material. The velocity can be calculated from output of the accelerometer in the following relationship,

$$v = g \int a dt = g \sum a \Delta t \quad (2)$$

where a is the instantaneous acceleration of striker expressed in g 's, and dt (or Δt) is a time step increment expressed in seconds. For this study, the Δt value used in the calculations is 2.6399×10^{-5} seconds. Figure 2 shows a typical velocity versus time plot. It can be observed in figure 2 that the striker's velocity increases initially until impact then reaches a local minimum value as the resistance of the specimen decreases. The point in time



Figure 1. Experimental setup.

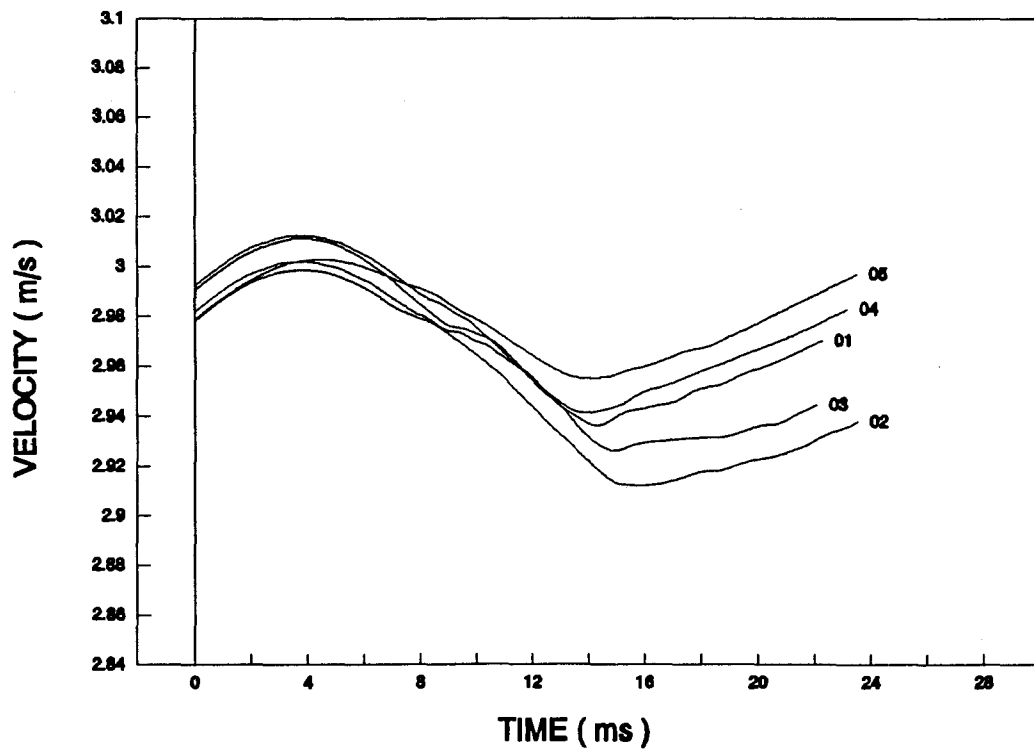


Figure 2. Typical velocity versus time plot.

at which the specimen's resistance has decreased significantly, the local minimum in striker velocity, has been defined as the end of the impact event for computational purposes.⁽³⁾ The total energy (E_t), therefore, has been defined as the energy at that point in time where the velocity reaches a local minimum value. Under this assumption, effects outside the impact event (specimen falling off the supports, friction forces, etc.) are neglected in the determination of E_t .⁽³⁾

The instantaneous load of the specimen during the impact event can also be calculated. The equation,

$$P = w_w a \quad (3)$$

is used to determine the instantaneous resistance of the specimen where w_w is the weight of the striker and a is the instantaneous acceleration of the striker expressed in g's. To compute the instantaneous energy absorbed by the specimen at any time during the impact event, the relationship,

$$E = \int P v dt = \sum P v \Delta t \quad (4)$$

is used.⁽³⁾

Analysis of Impact Test Data

Beginning in the early 1970's, there have been several instrumented impact test studies that have determined the critical impact test parameters for the analysis of test data.⁽⁵⁻⁷⁾ The points to consider on the corresponding load and energy curves are: the initiation load, the initiation energy, the maximum load, the energy at the maximum load, and the total energy absorbed by the impacted specimen.⁽³⁾ Figure 3 illustrates the important data analysis points. From the impact point (time = 0 ms) until initiation load (P_1), purely elastic initiation energy (E_1) is retained by the material while in flexure. While in this phase, no gross material failures occur, although failures on the microscopic level [e.g., buckling of fibers on the top surface (compression side) and debonding of the interface between the fibers and matrix material on either the compression or the tension side] may occur.⁽⁷⁾ When the test specimen reaches the initiation load, tensile failures (fiber failures) and shear failures (interlaminar) or both will begin to originate. Following this point, the failure will proceed in one of two failure mechanisms. Either the fracture propagates in a catastrophic (brittle-like) manner or in a non-catastrophic (ductile-like) manner.⁽³⁾ For a catastrophic failure, the failure mode is very abrupt resulting in an initiation load point (P_1) and a maximum load point (P_m), which are identical in time. For a non-catastrophic failure, the fiber breakage is characterized by load oscillations that can remain essentially steady or can drift up or drift down.⁽⁸⁾ This type of failure is less sudden, resulting in distinct initiation load (P_1) and maximum load (P_m) points. Quite often, a superposition of the two modes occur. In this case, the initiation load point is followed by load oscillations until the specimen suddenly fails.⁽³⁾ This blend of two failure modes is portrayed in figure 3. Referring to this figure, it can be seen that the initiation load and the maximum load points are separate points as in the non-catastrophic failure mechanism. Fiber failures occur in the center

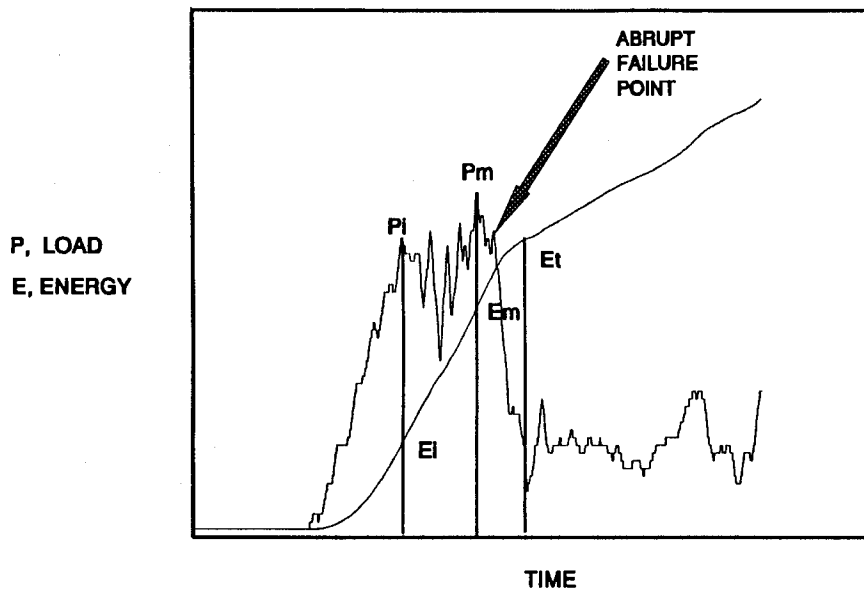


Figure 3. Important data analysis points.

plateau region until an abrupt shear failure (represented by the sharp drop in load level on the curve) occurs.

CHAPTER 3. IMPACT TESTS ON PULTRUDED COMPOSITE MATERIALS

Test Specimens

The test specimens were cut from three standard types of pultruded sections made by Creative Pultrusions, Inc. in Alum Bank, Pennsylvania. These were: channels (LV2, LP3, TP3 - all of which were cut from the web), I-beams (TV3-web, LV3-flange), and plates (LV4, TV4). All of the material tested contained alternating layers of unidirectional fibers and layers of continuous-strand mat. In addition, there was a polymeric surface veil on the top and bottom layers that provided a smooth outer surface.⁽³⁾ The test specimens were named according to a three-character nomenclature. The first character was a letter that signified the orientation of the majority of the fibers present. Specimens with fiber rovings in the longitudinal direction were denoted by an "L" and specimens with fiber rovings in the transverse direction were denoted by a "T". The second letter referred to the matrix material, either vinyl ester (V) or polyester (P). The third character was a number referring to the specimen thickness given in eighths of an inch. For example, a "2" refers to 2/8 in. The thicknesses in SI units were as follows: 2 = 6.35 mm, 3 = 9.56 mm, and 4 = 12.7 mm. Every test specimen had a nominal width of 25.4 mm (1.0 in) and ranged in nominal length from 159 to 210 mm (6.25 to 8.25 in). Five of each specimen type (only four LV4 specimens) were tested. Table 1 presents the test specimen specifications for the series of impact tests on pultruded material.

Test Results

The load versus time curves for each test grouped according to specimen type are presented in figures 4 through 10. The energy versus time curves are shown in figures 11 through 17. Averaging each point in time from the load versus time and energy versus time curves for each specimen type, a single average curve is plotted. These are depicted in figures 18 through 24 for the average load and figures 25 through 31 for the average energy. Also, the average load plus and minus one standard deviation is plotted as figures 32 through 38. For clarity, the average load curve is not plotted with the standard deviation in figures 32 through 38.

To compare test results for load and energy from different size specimens, normalized results have been used. Previous studies on impact testing have normalized the load and energy responses by dividing by the cross-sectional area at the point of impact.^(3,4) Since it has been generally accepted for use in prior studies, normalizing by cross-sectional area is used initially in this study. Figures 39 and 40 illustrate normalization by cross-sectional area for load and energy respectively. Data is taken from the average load and energy curves (see figures 18 through 31 and table 1) and is divided by the cross-sectional area to obtain the normalized plot.

Because the specimen is loaded in flexure it may be more appropriate to normalize by a bending parameter such as section modulus. The possibility for misleading results is the impetus for examining other normalization techniques that are described later. In aircraft applications, where weight is a primary concern, load and energy data is frequently normalized by the weight of the

Table 1. Test specimen specifications.

SAMPLE	MATRIX	SECTION CUT FROM	THICKNESS mm (in)	WIDTH mm (in)	% GLASS BY WT.
LV2	VINYL ESTER	CHANNEL WEB	6.4 (0.25)	25 (1.0)	40
LV3	VINYL ESTER	I-SEC FLANGE	9.6 (0.38)	25 (1.0)	50
LV4	VINYL ESTER	PLATE	12.7 (0.5)	25 (1.0)	<40
TV3	VINYL ESTER	I-SEC WEB	9.6 (0.38)	25 (1.0)	50
TV4	VINYL ESTER	PLATE	12.7 (0.5)	25 (1.0)	<40
LP3	POLYESTER	CHANNEL WEB	9.6 (0.38)	25 (1.0)	50
TP3	POLYESTER	CHANNEL WEB	9.6 (0.38)	25 (1.0)	50

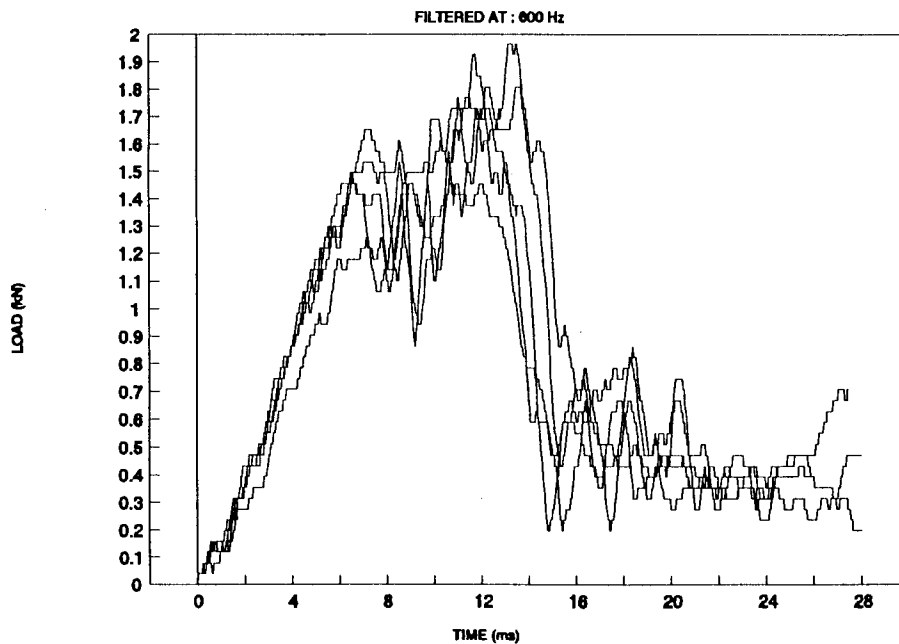


Figure 4. Load versus time (LV2).

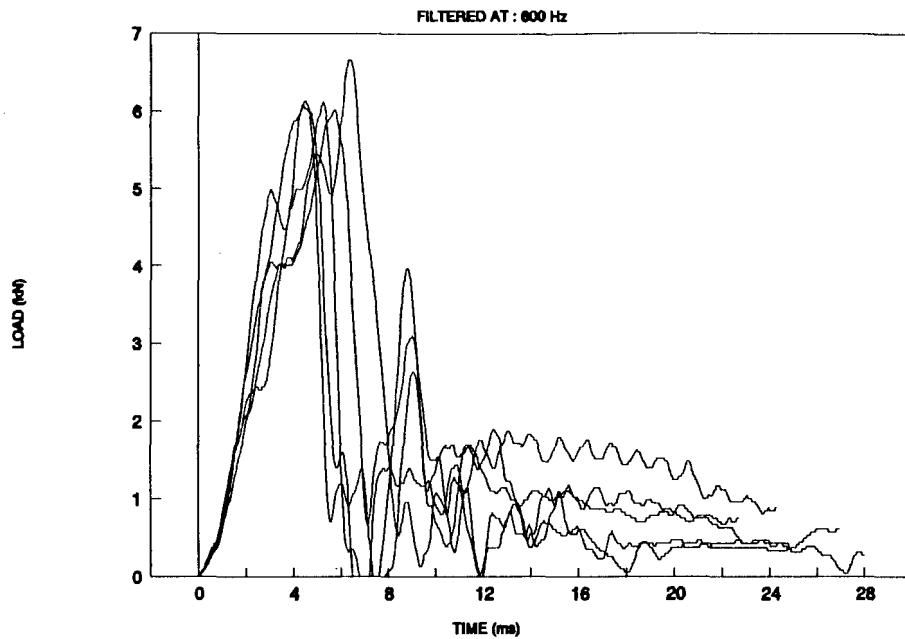


Figure 5. Load versus time (LV3).

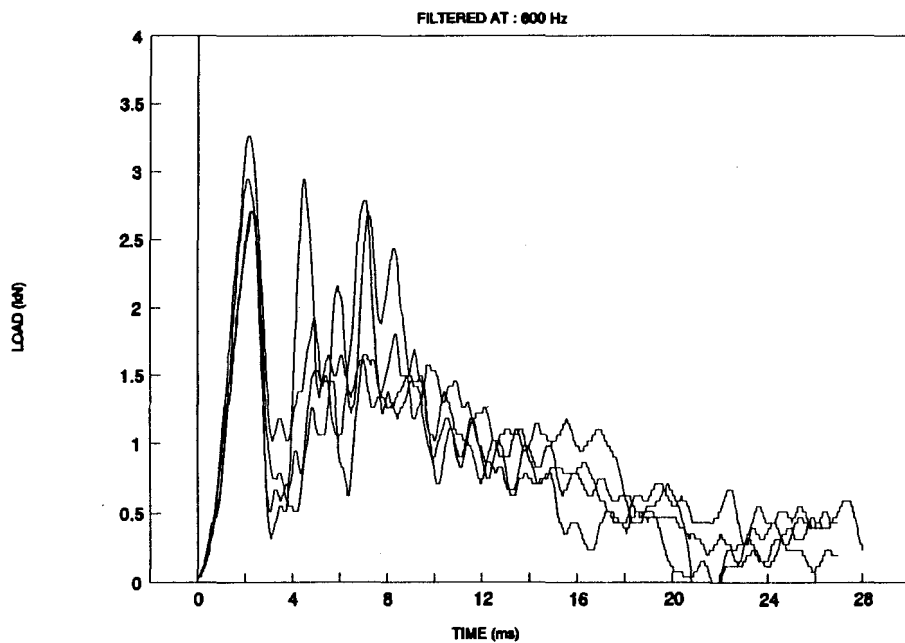


Figure 6. Load versus time (LV4).

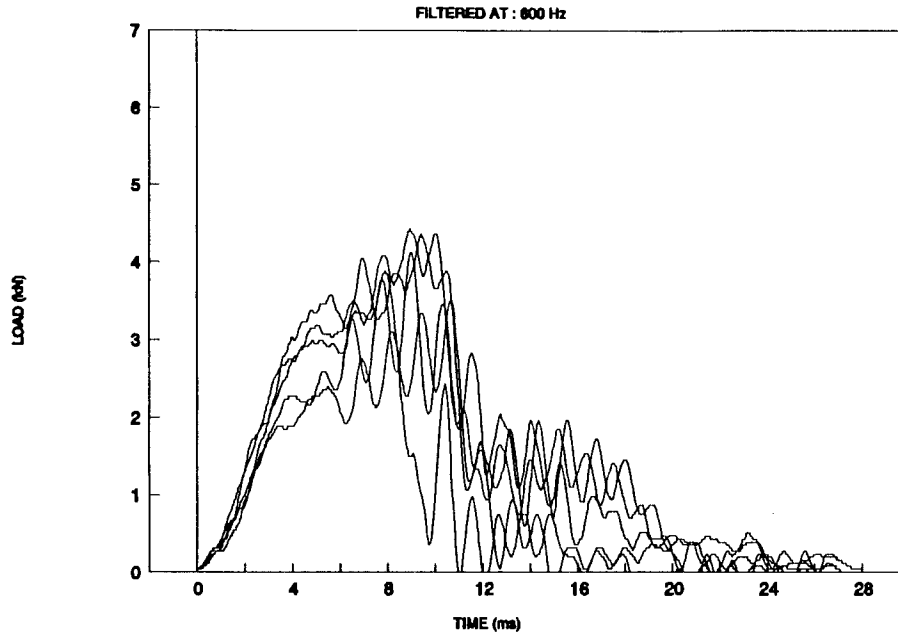


Figure 7. Load versus time (LP3).

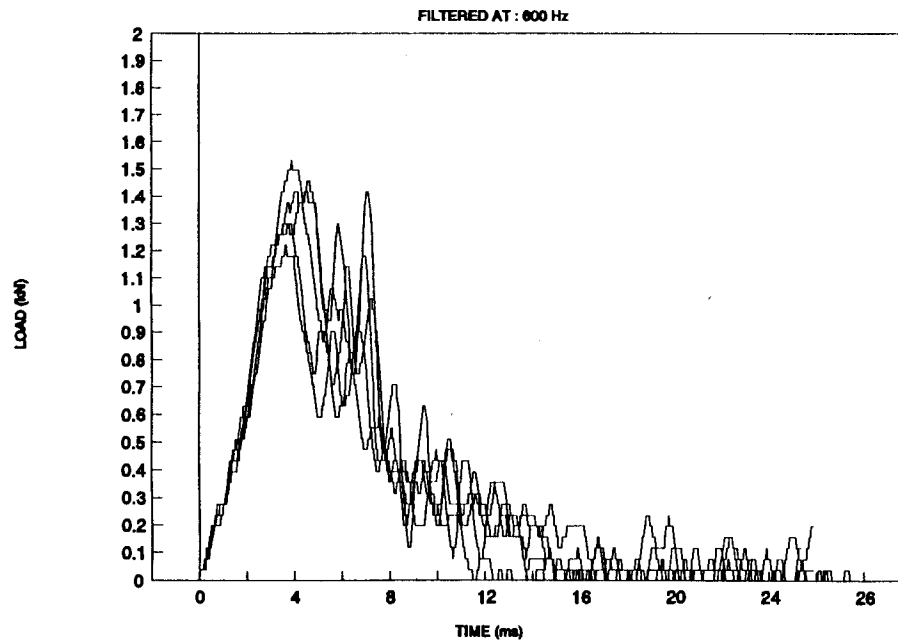


Figure 8. Load versus time (TP3).

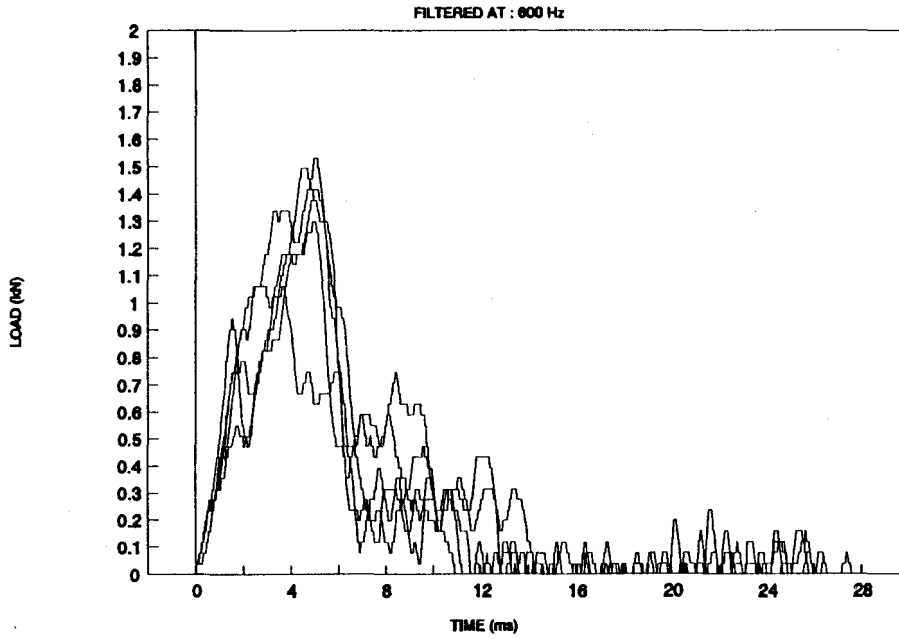


Figure 9. Load versus time (TV3).

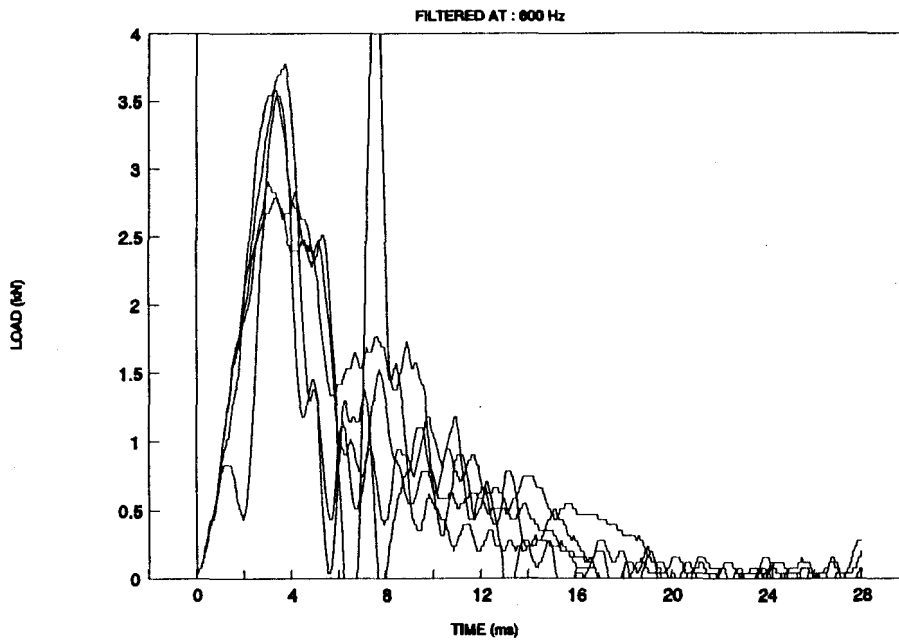


Figure 10. Load versus time (TV4).

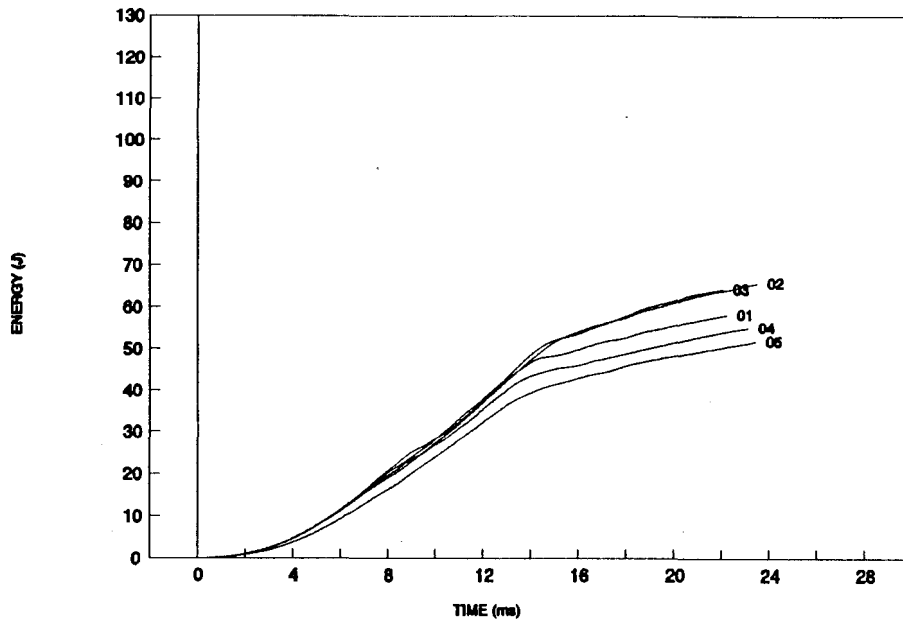


Figure 11. Energy versus time (LV2).

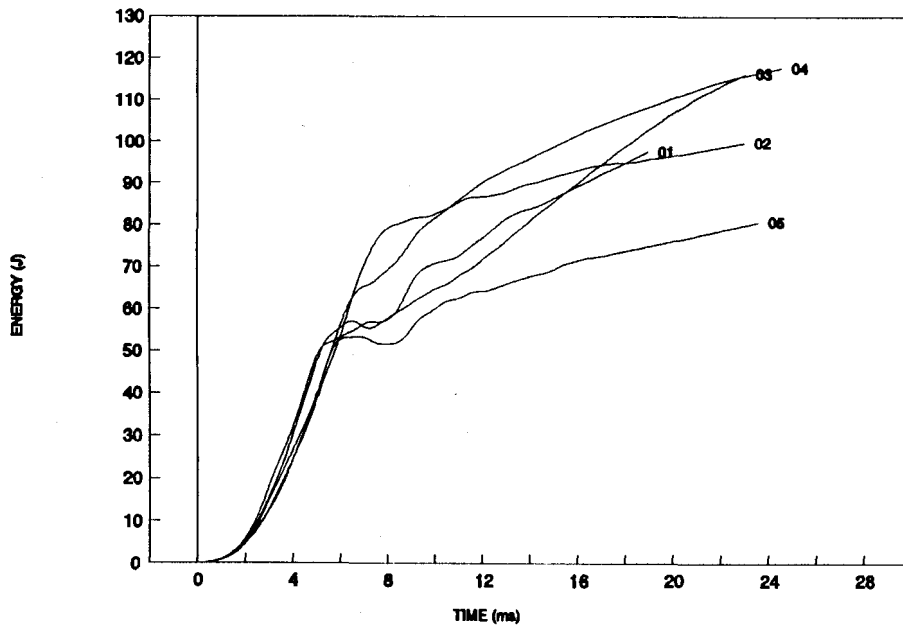


Figure 12. Energy versus time (LV3).

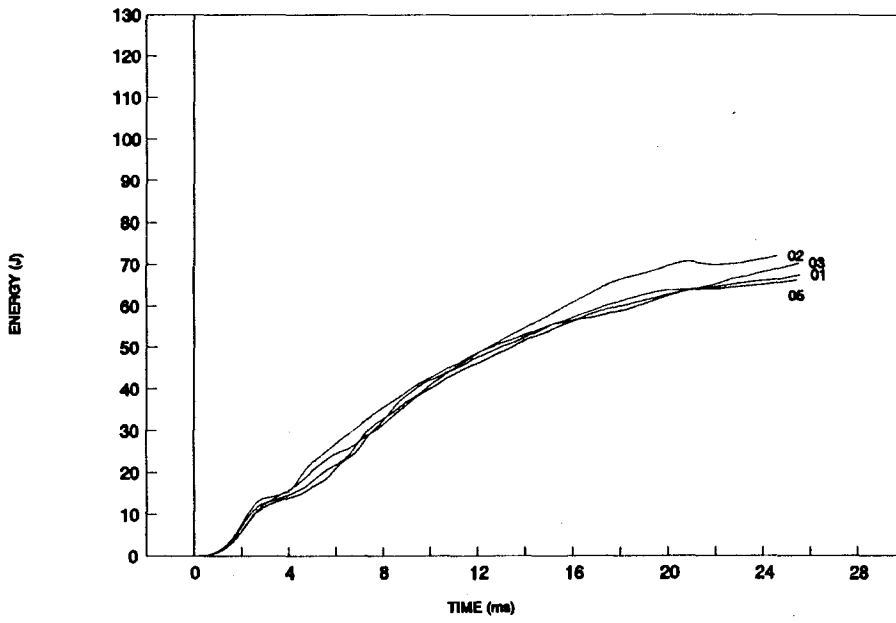


Figure 13. Energy versus time (LV4).

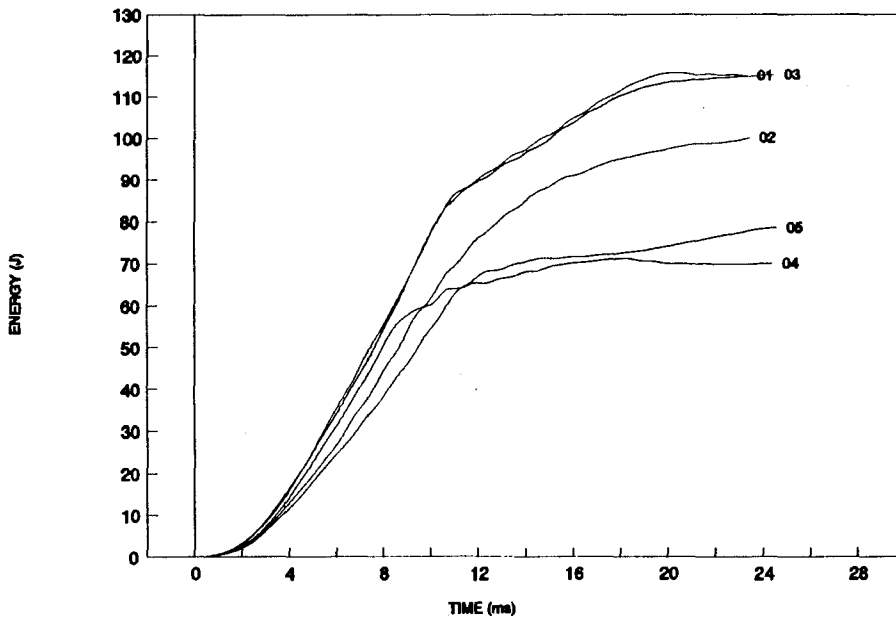


Figure 14. Energy versus time (LP3).

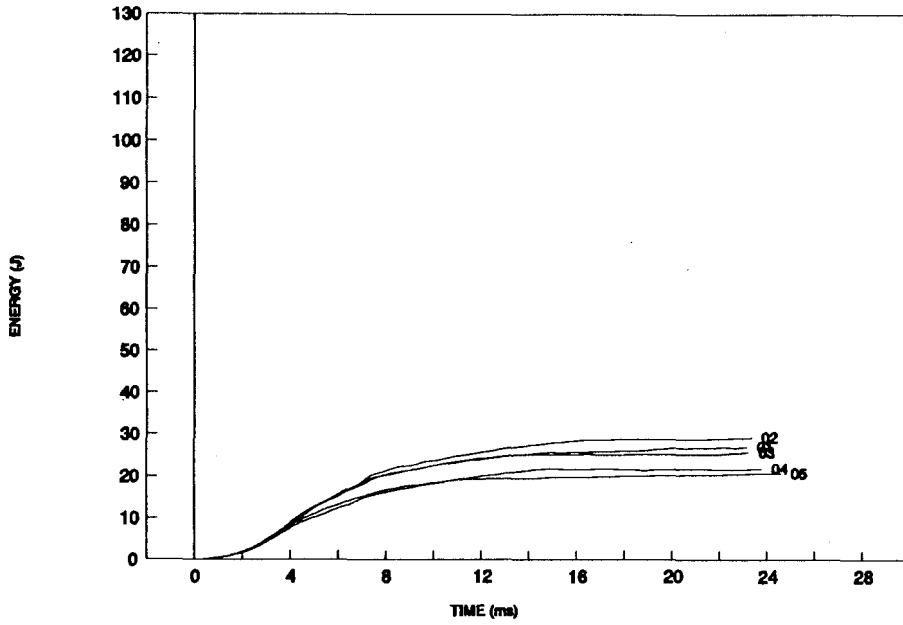


Figure 15. Energy versus time (TP3).

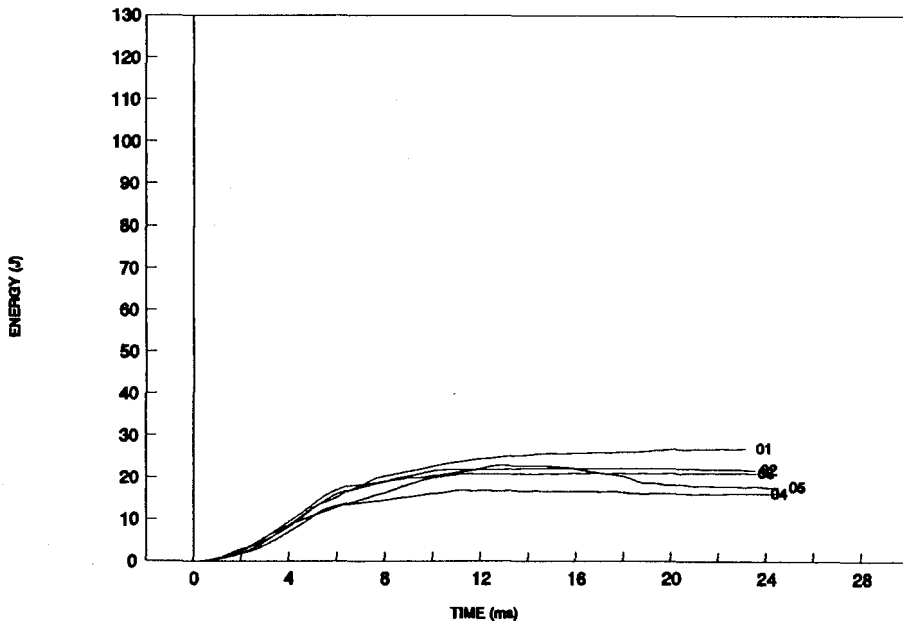


Figure 16. Energy versus time (TV3).

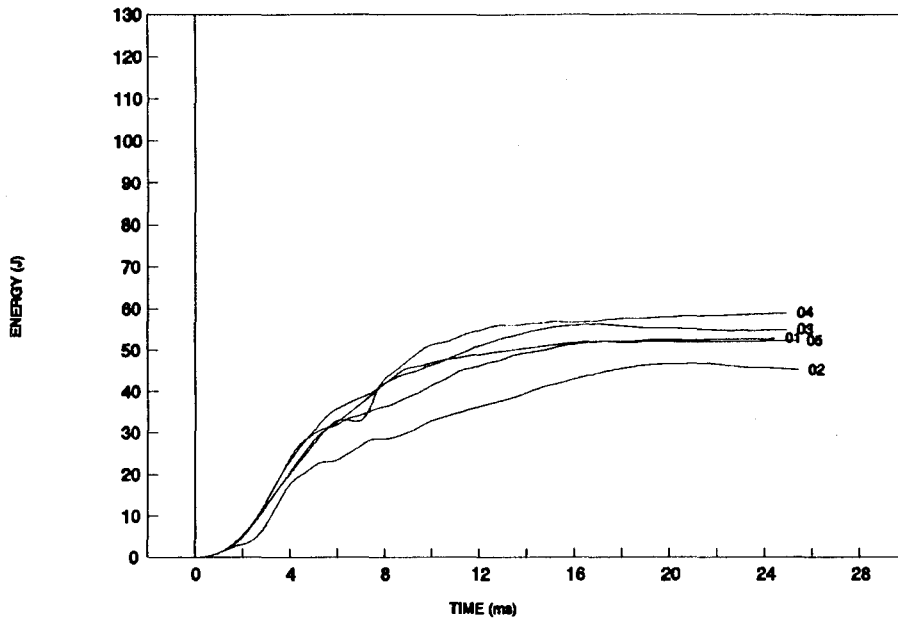


Figure 17. Energy versus time (TV4).

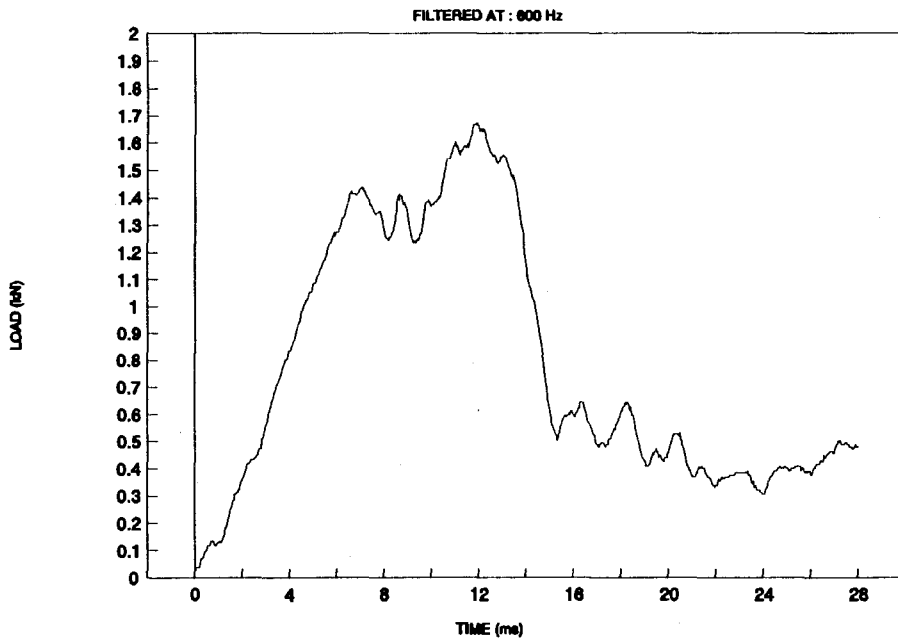


Figure 18. Average load versus time (LV2).

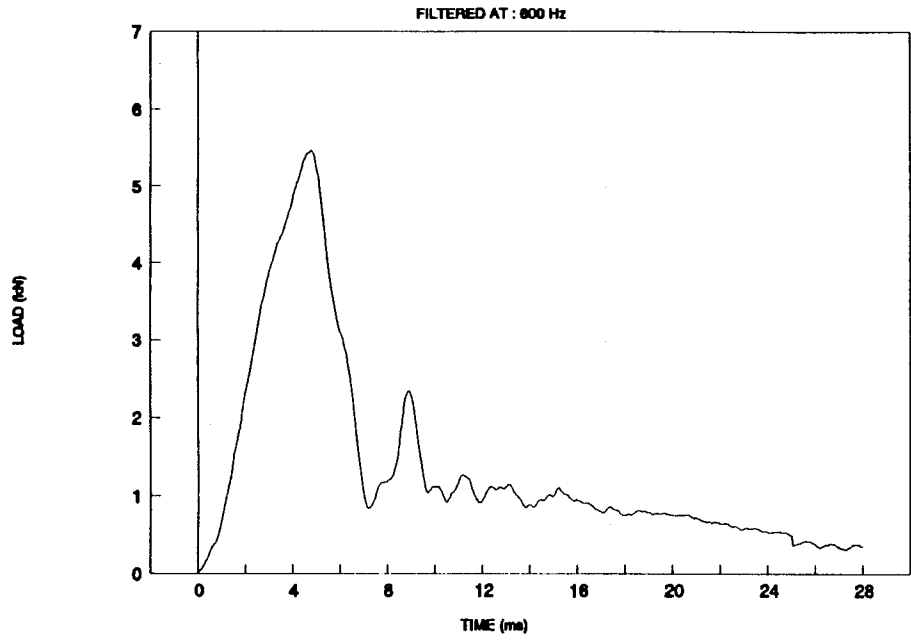


Figure 19. Average load versus time (LV3).

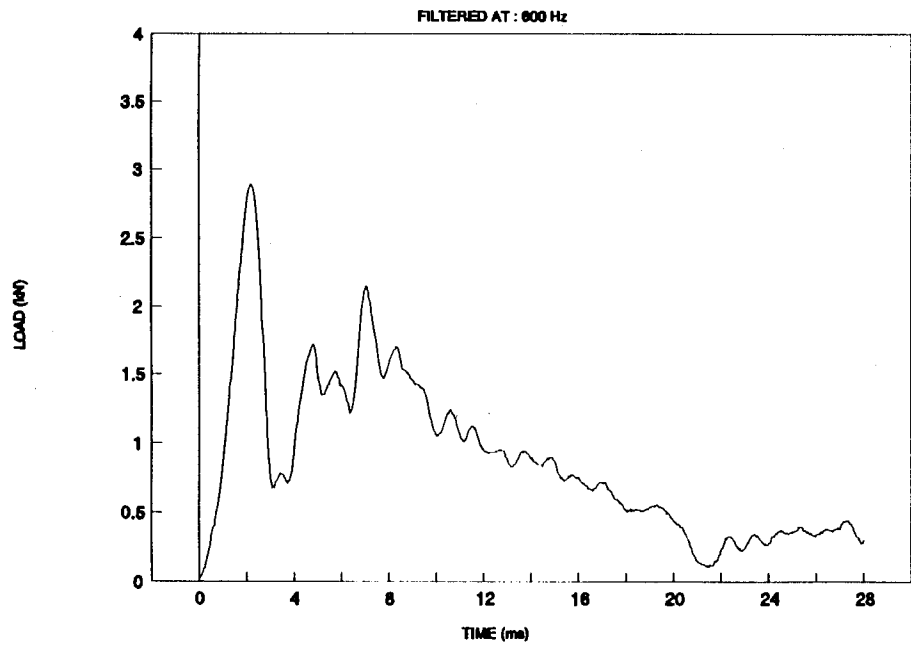


Figure 20. Average load versus time (LV4).

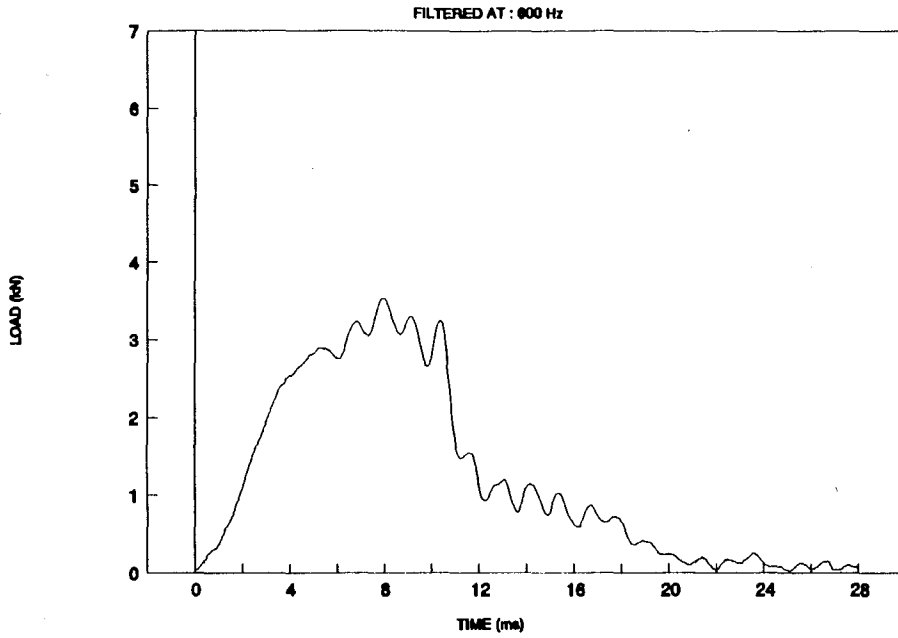


Figure 21. Average load versus time (LP3).

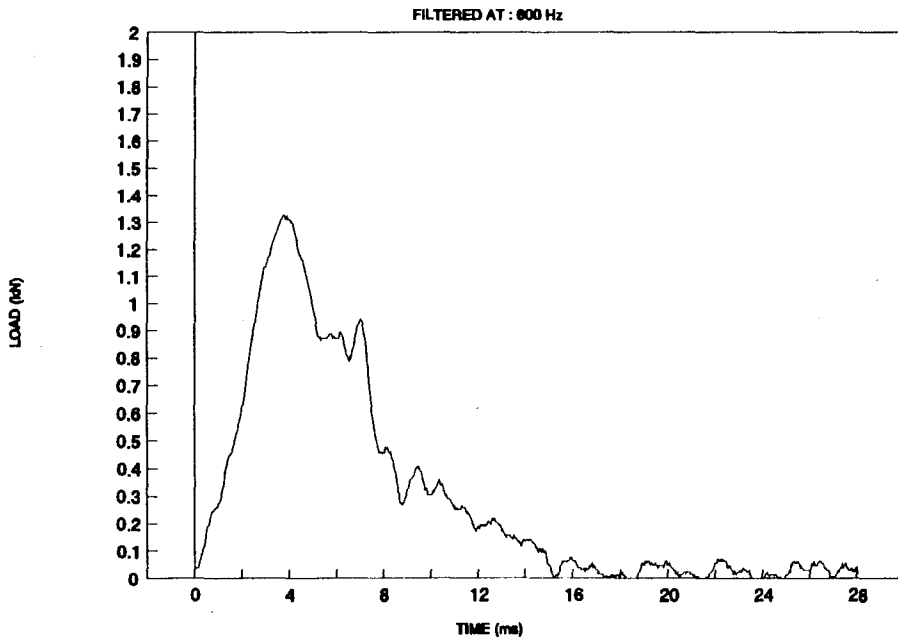


Figure 22. Average load versus time (TP3).

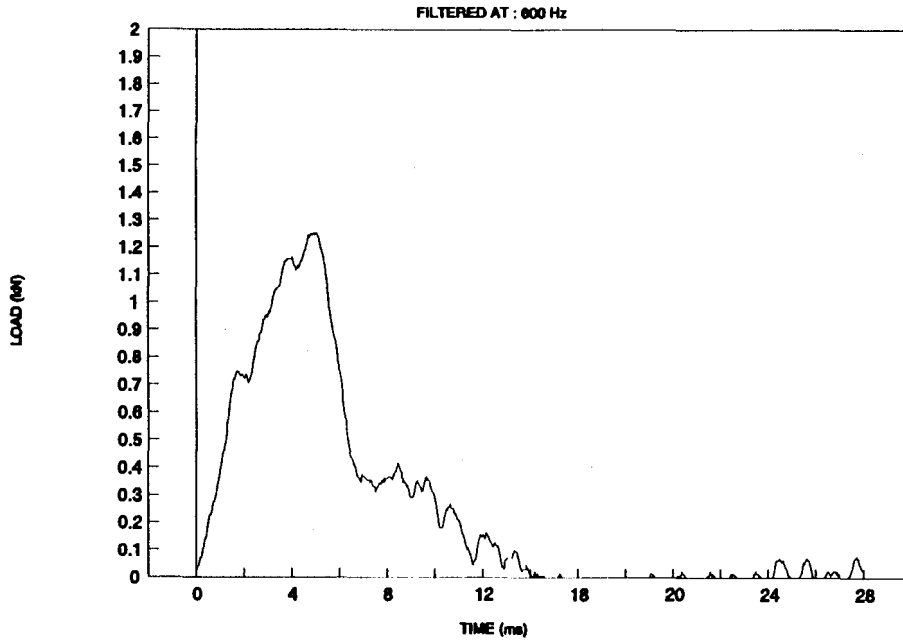


Figure 23. Average load versus time (TV3).

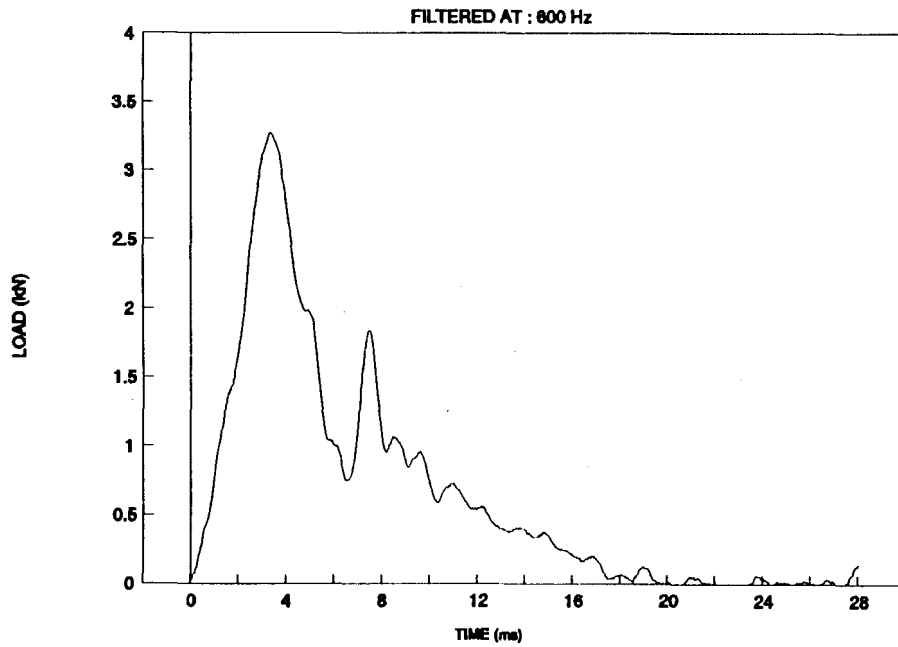


Figure 24. Average load versus time (TV4).

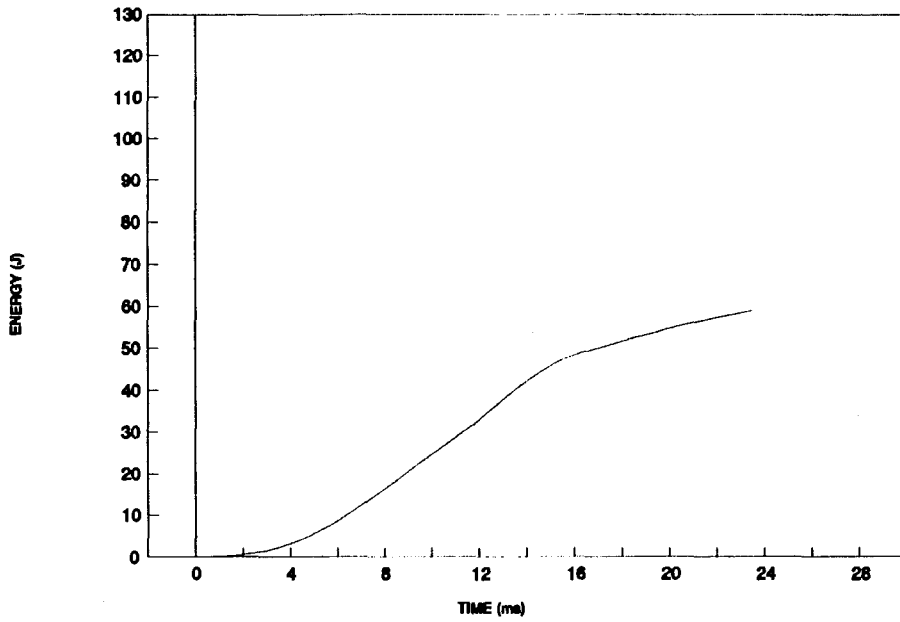


Figure 25. Average energy versus time (LV2).

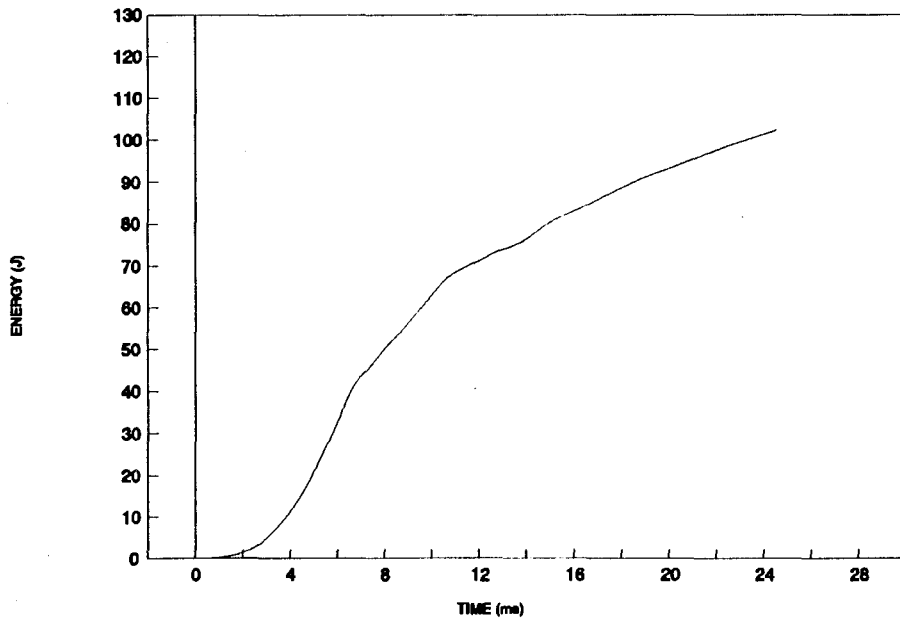


Figure 26. Average energy versus time (LV3).

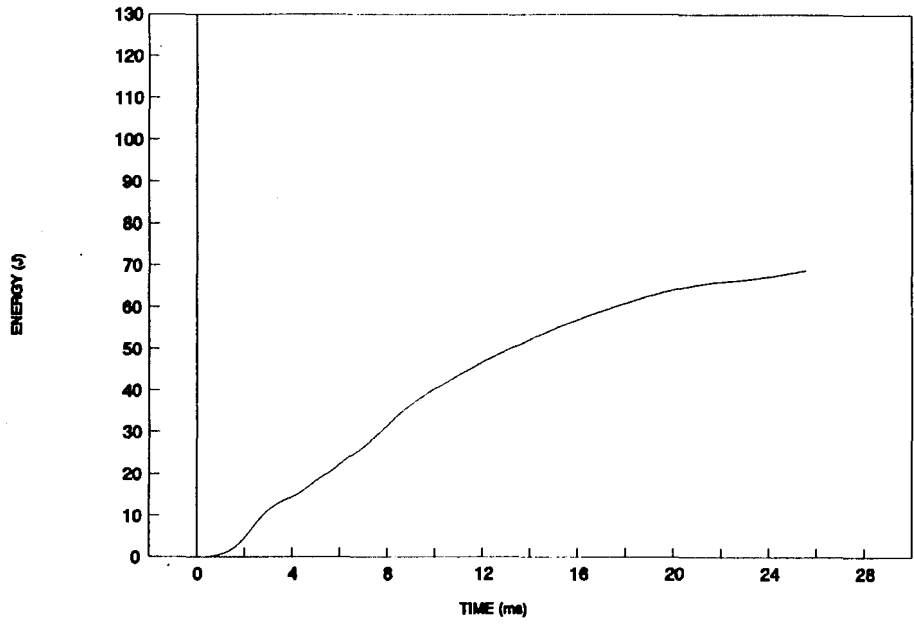


Figure 27. Average energy versus time (LV4).

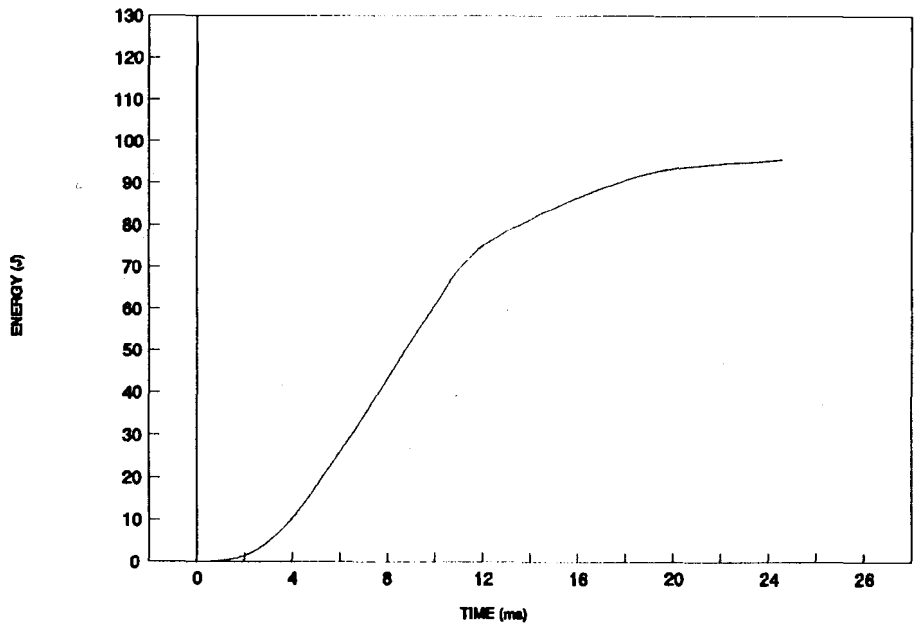


Figure 28. Average energy versus time (LP3).

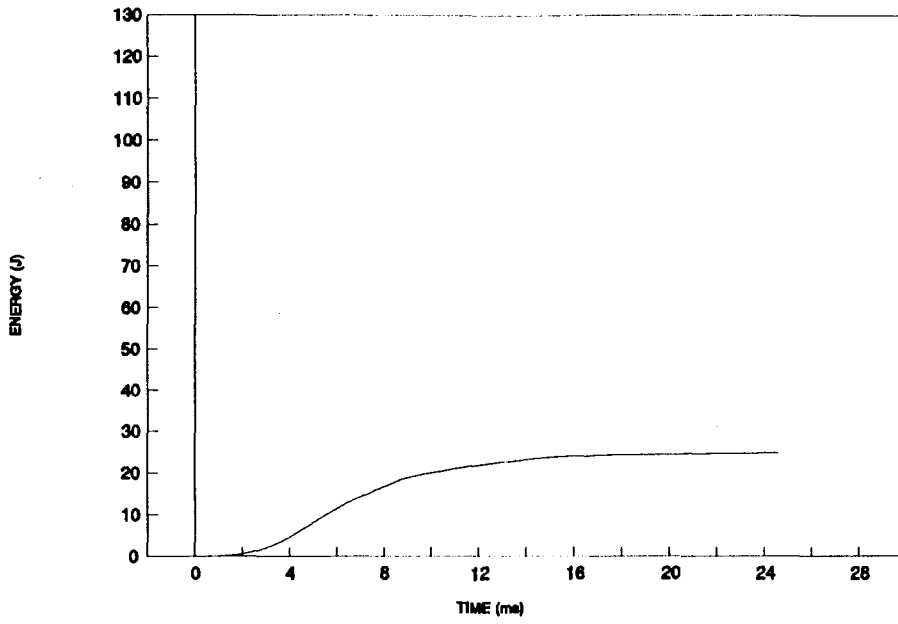


Figure 29. Average energy versus time (TP3).

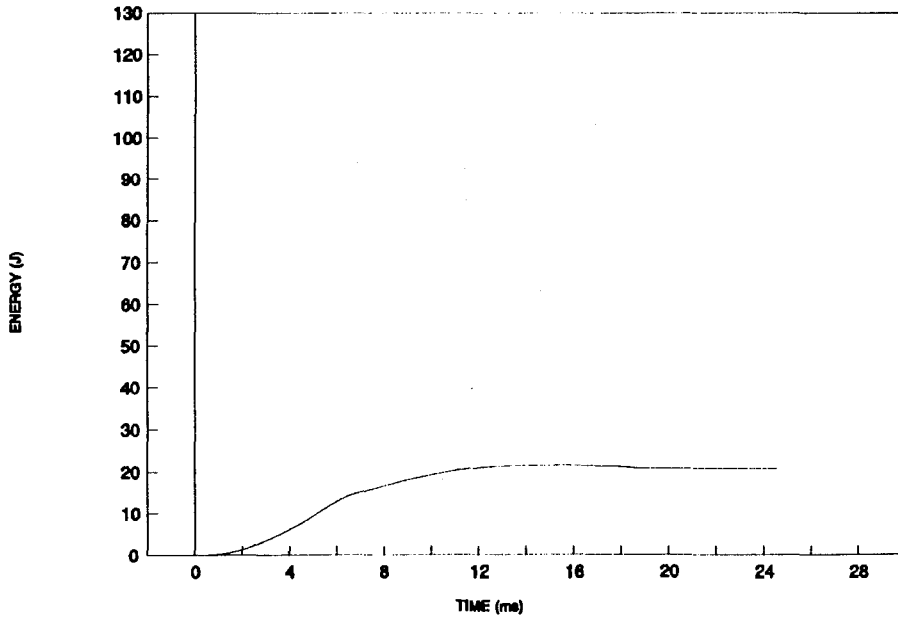


Figure 30. Average energy versus time (TV3).

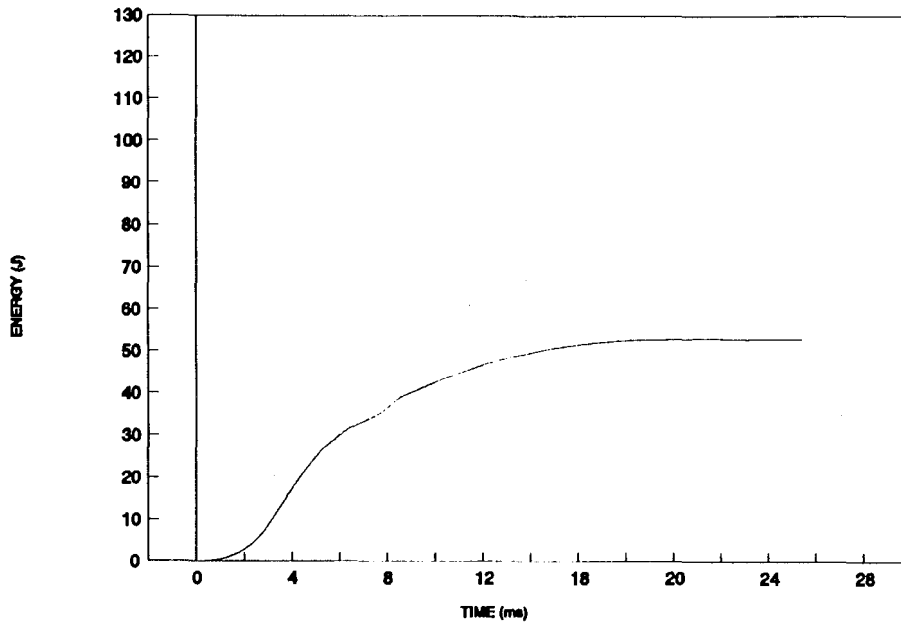


Figure 31. Average energy versus time (TV4).

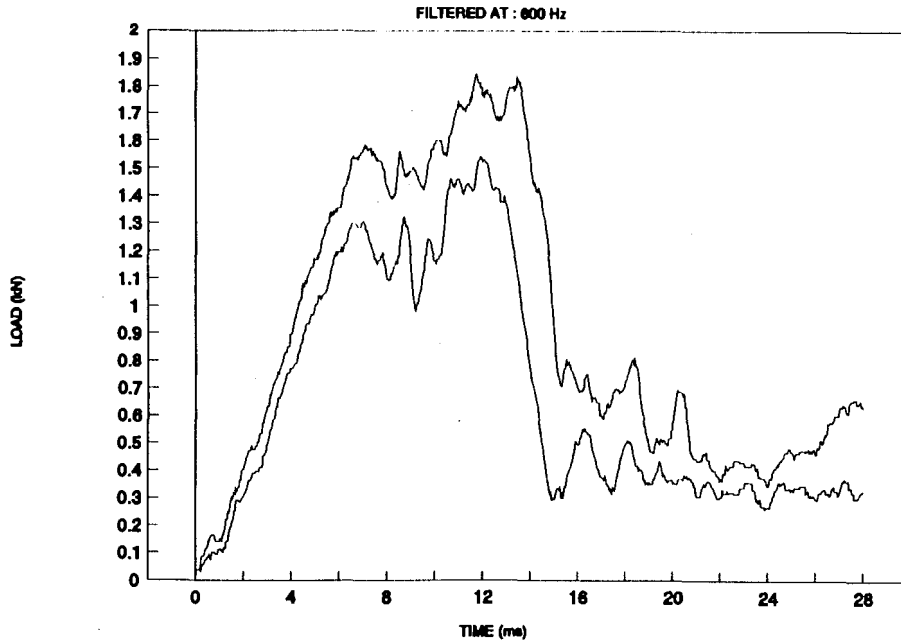


Figure 32. Standard deviation (LV2).

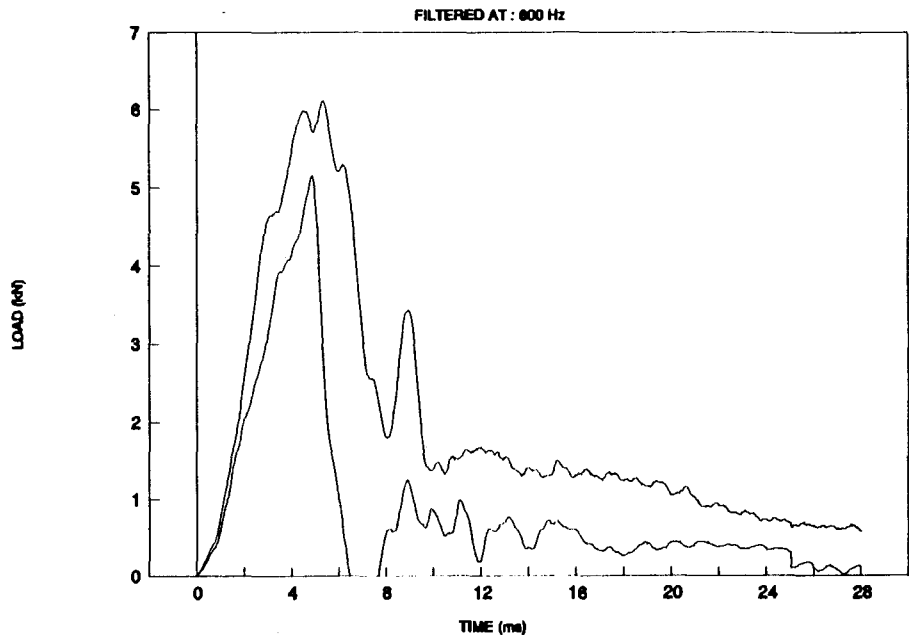


Figure 33. Standard deviation (LV3).

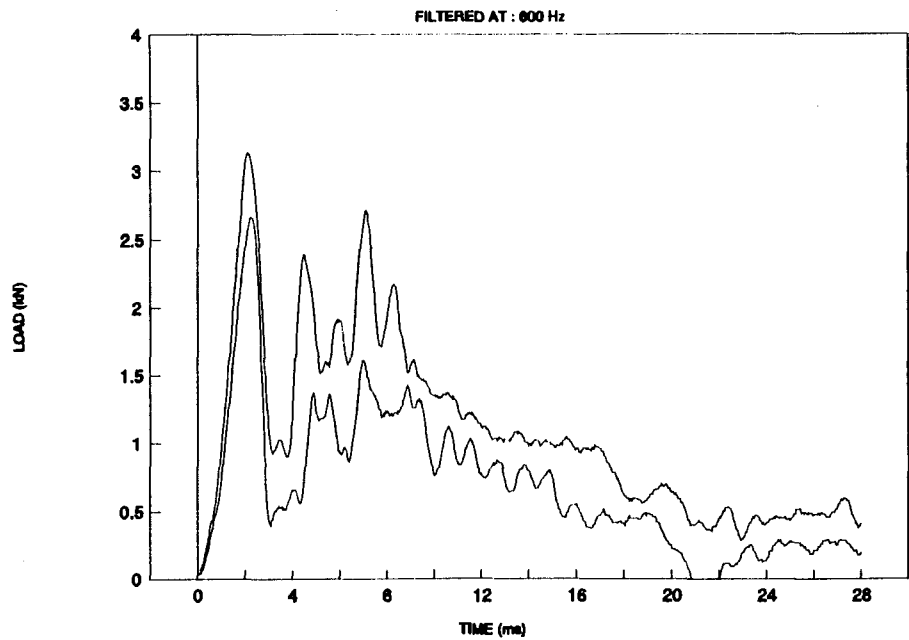


Figure 34. Standard deviation (LV4).

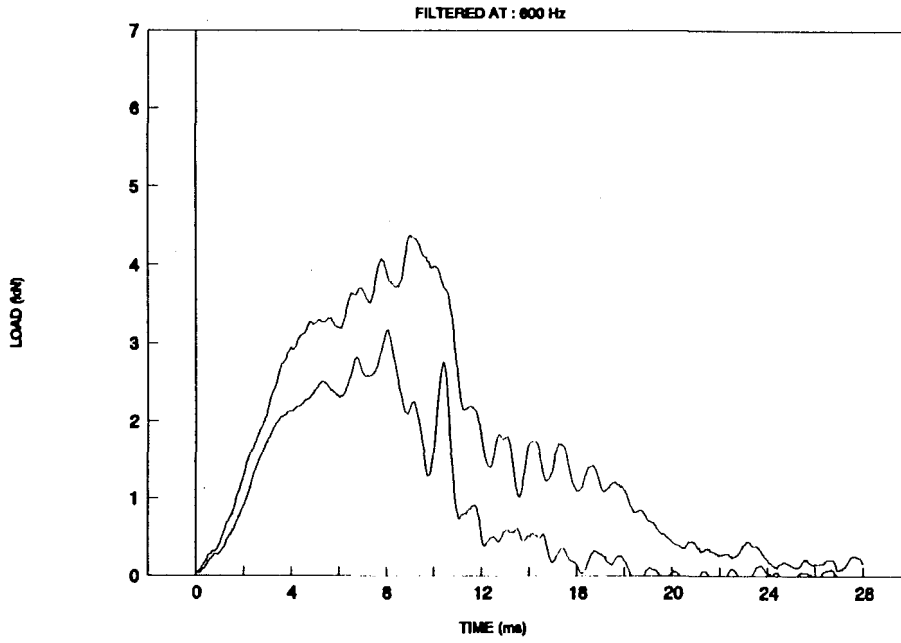


Figure 35. Standard deviation (LP3).

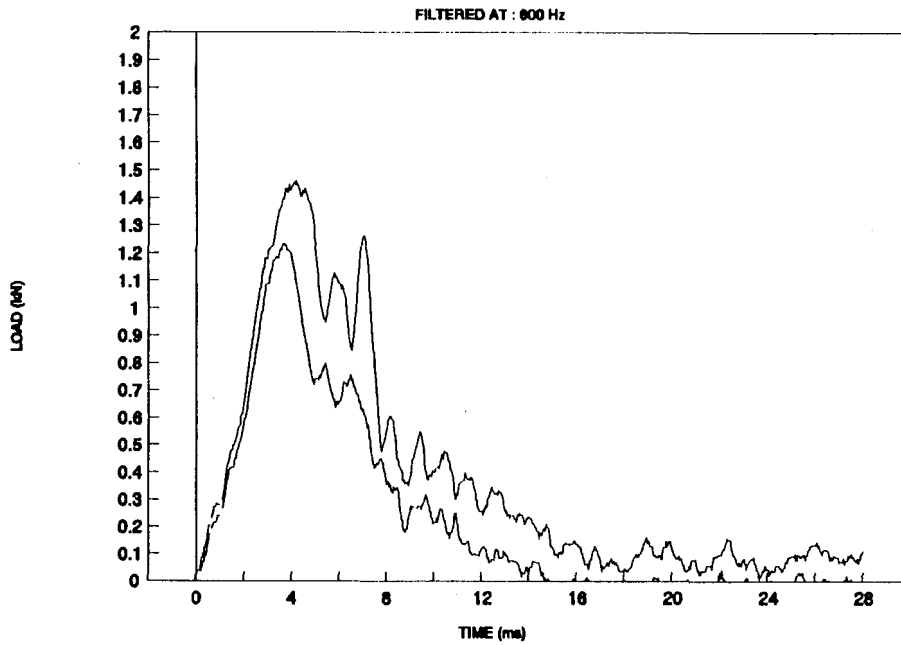


Figure 36. Standard deviation (TP3).

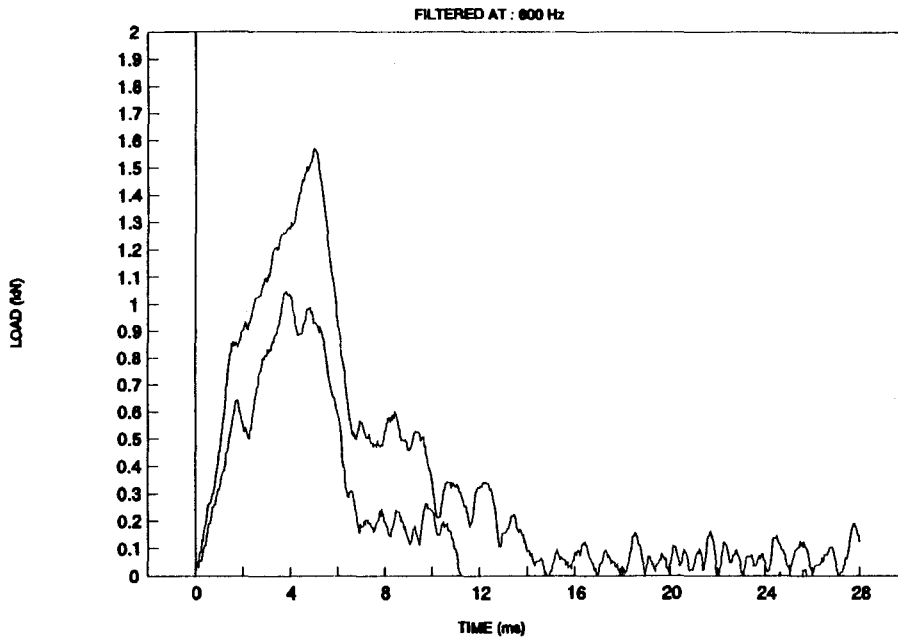


Figure 37. Standard deviation (TV3).

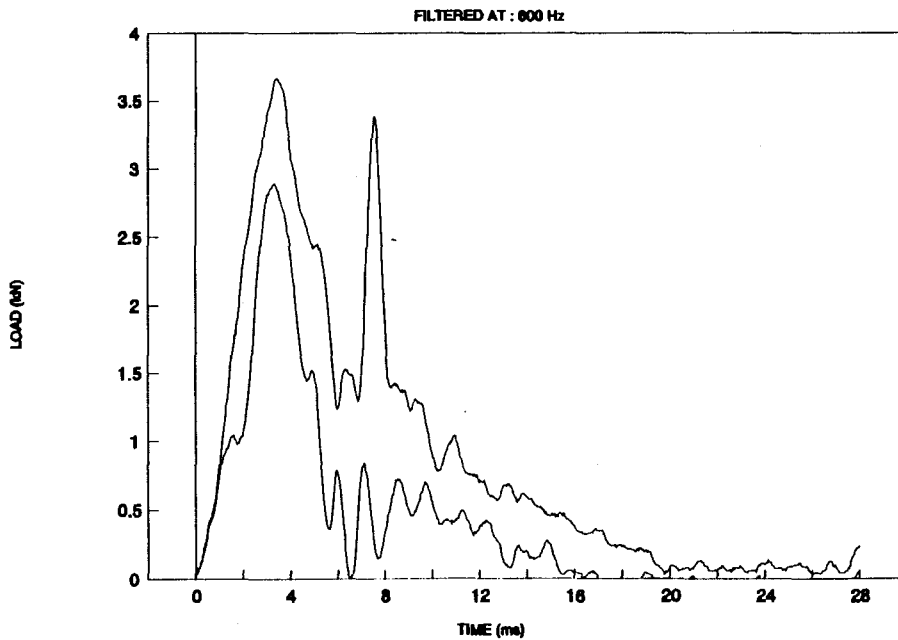


Figure 38. Standard deviation (TV4).

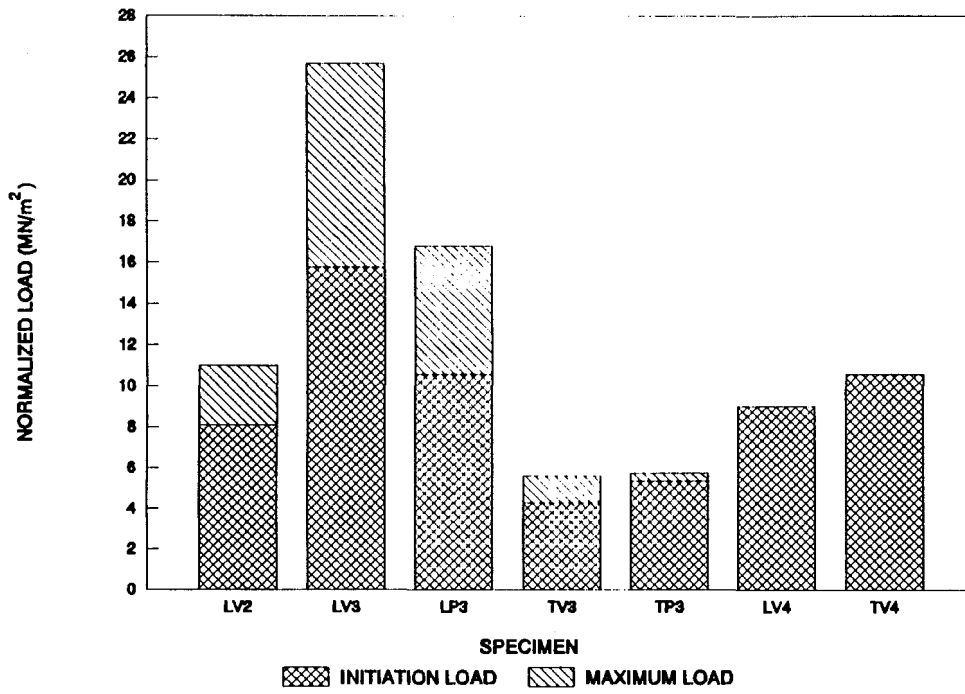


Figure 39. Normalized load (by area) - pultruded.

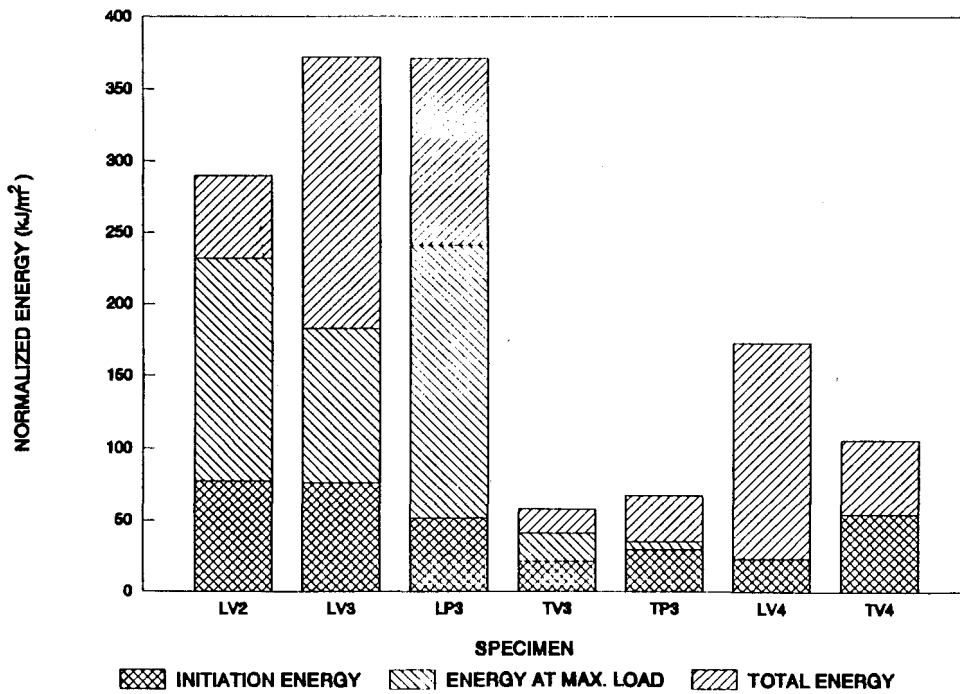


Figure 40. Normalized energy (by area) - pultruded.

specimen.⁽⁹⁾ For roadside safety structures, however, this would not be practical since very little consideration is given to the weight of a roadside structure. Considering a beam under three-point loading, the maximum elastic bending stress (σ_e) can be represented by the relationship,

$$\sigma_e = Mc/I_z \quad (5)$$

where M is the maximum bending moment at each point in time ($M = PL/4$), c is the distance from the neutral axis to the outermost surface (for a rectangular cross-sectional area, $c = h/2$), and I_z is the moment of inertia of the cross-sectional area.⁽¹⁾ Therefore, the maximum elastic stress can be represented by the equation,

$$\sigma_e = PLh/8I_z \quad (6)$$

where P is the instantaneous load, L is the span length, and h is the thickness of the cross section. Thus, this relationship ($Lh/8I_z$) can be used to normalize the quantity. The normalized values by all geometric parameters are presented in bar charts for the normalized load in figure 41 and the normalized energy in figure 42. This normalization technique has been used for all subsequent tests and gives results that are consistent with expectations of the material.

Table 2 presents the average load and energy points for the important data analysis points. These points are taken from the average load and energy versus time curves (figures 18 through 31). Using the average curves as a single data analysis curve simplifies the data analysis of test specimens of a specific type. In other words, an overall representation of several impact test records can be analyzed as a single curve. This process is similar to locating the specific points on the individual curves and averaging these points with some exceptions. If the average curve changes the nature (or shape) of a curve for a particular specimen type (i.e., the individual curves have features that the average curve does not), then the selection of a point on the average curve will differ from the points on the respective individual curves for that specimen type. As an example of this, figure 5 shows the individual load versus time curves for the LV3 specimen and figure 19 shows the LV3 average load versus time. Comparing the two figures, it is noted that some of the individual LV3 curves have distinct initiation load and maximum load points, while in the average load versus time curve these points are coincidental. This can be interpreted for the most part, as the LV3 specimen has an abrupt failure, but experimentally, a few specimens exhibit load versus time curves with distinct initiation and maximum loads. This will lead to a misleading result if points from individual curves are taken and averaged since the predominant failure mechanism is shear failure. Using the average curve thereby eliminates the discrepancies caused by a rarely occurring phenomenon, such as a distinct initiation load and maximum load points for LV3 specimens. This method also takes into account the scatter in time at which points during the impact event occur. For example, the maximum load for every test specimen of a particular type occurred at a different instant in time. When these curves are averaged, the maximum peak will generally be lower than averaging individual points because the maxima are scattered in time. This is the case for the energy curves as well. Thus, by obtaining a slightly lower

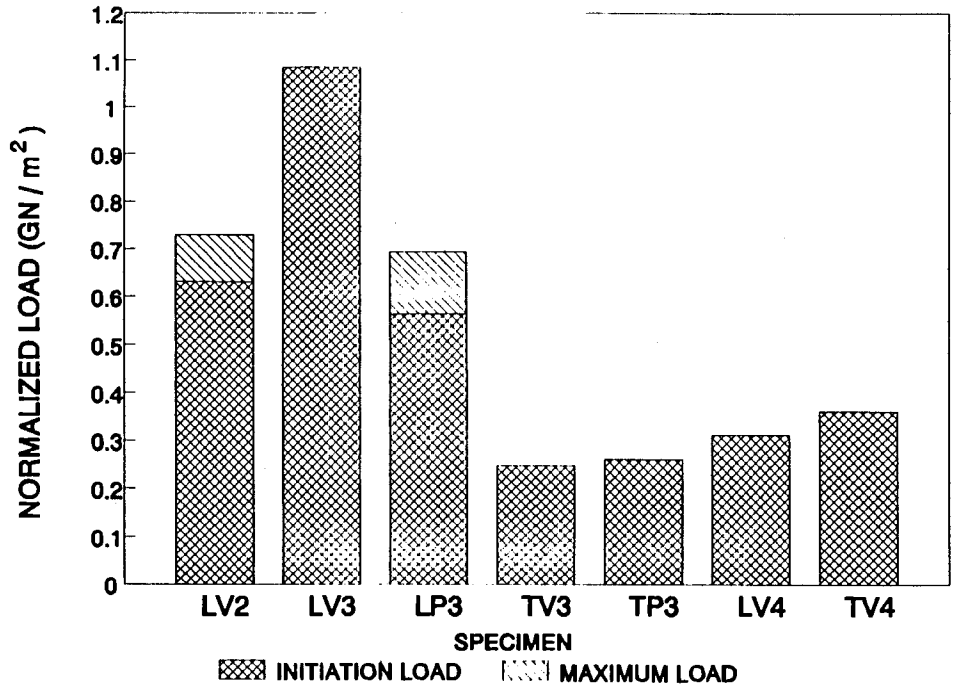


Figure 41. Normalized load (by all geometry) - pultruded.

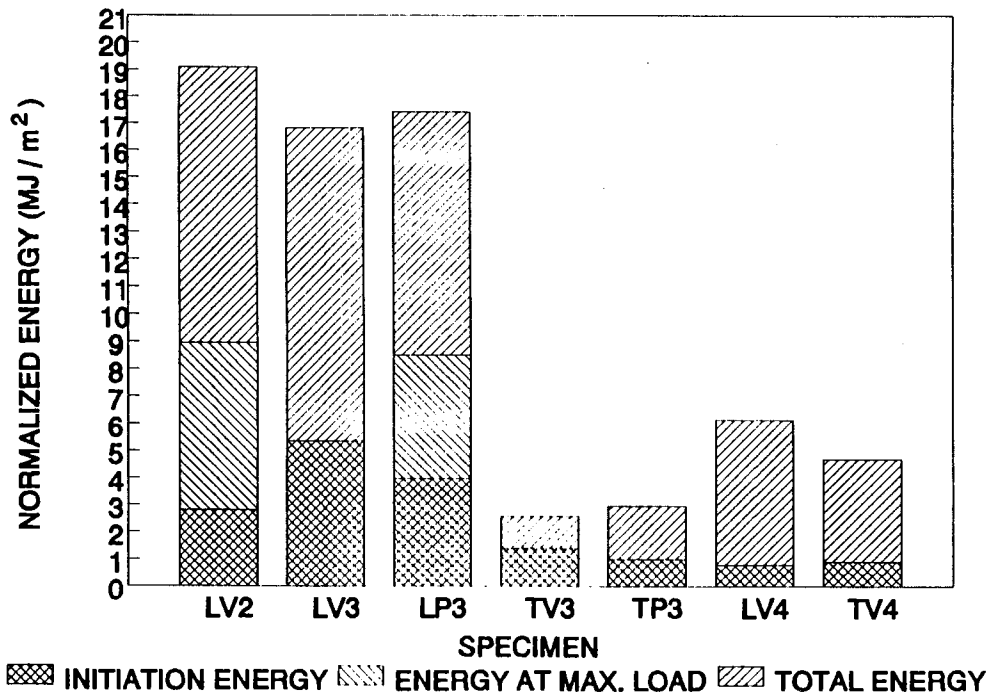


Figure 42. Normalized energy (by all geometry) - pultruded.

Table 2. Average values.

SPECIMEN	LV2	LV3	LV4	TV3	TV4	LP3	TP3
INITIATION LOAD, N	1313	5491	2911	1258	3258	2556	1299
lb	296	1234	654	283	732	575	292
INITIATION ENERGY, J	11.1	26.9	7.0	6.9	8.0	20.0	5.1
ft-lb	8.2	20	5.2	5.1	5.9	15	3.8
MAXIMUM LOAD, N	1778	5491	2911	1258	3258	4067	1299
lb	400	1234	654	283	732	914	292
ENERGY AT MAX LOAD, J	38.0	26.9	7.0	6.9	8.0	43.0	5.1
ft-lb	28	20	5.2	5.1	5.9	32	3.8
TOTAL ENERGY, J	43.1	84.9	55.2	14.0	41.9	88.0	16.3
ft-lb	32	63	41	10	31	65	12

maximum, this method yields a conservative answer (i.e., a reported value that is somewhat lower than the actual value).

Comparing the average load versus time curves for the LV3, LV4, and LP3 specimens (figures 19 through 21) with high-speed film results from these tests (figures 43 through 45), two different failure mechanisms are noted. In the first mechanism, fibers begin to fail in tension along the bottom face of the specimen. This is followed by the failure changing into a shear-type failure with cracks propagating along the length of the specimen. This is the case for the LV3 and LP3 specimens [at approximately 6 ms for the LV3 specimen (figure 43) and at approximately 7 ms for the LP3 specimen (figure 45)]. The second type of failure mechanism is seen in the thicker LV4 specimens (figures 20 and 44). In this case, the specimen first develops a shear failure at or near the beam's neutral axis (at approximately 3 ms). A tension failure subsequently occurs (at 9 ms) after the specimen has lost some of its resistance.⁽¹⁾ This type of failure mechanism is also exhibited by all of the primarily transverse fiber specimens (TV3, TV4, and TP3) and the LV4 specimens. The LV4 specimens are the exception, as the other longitudinal

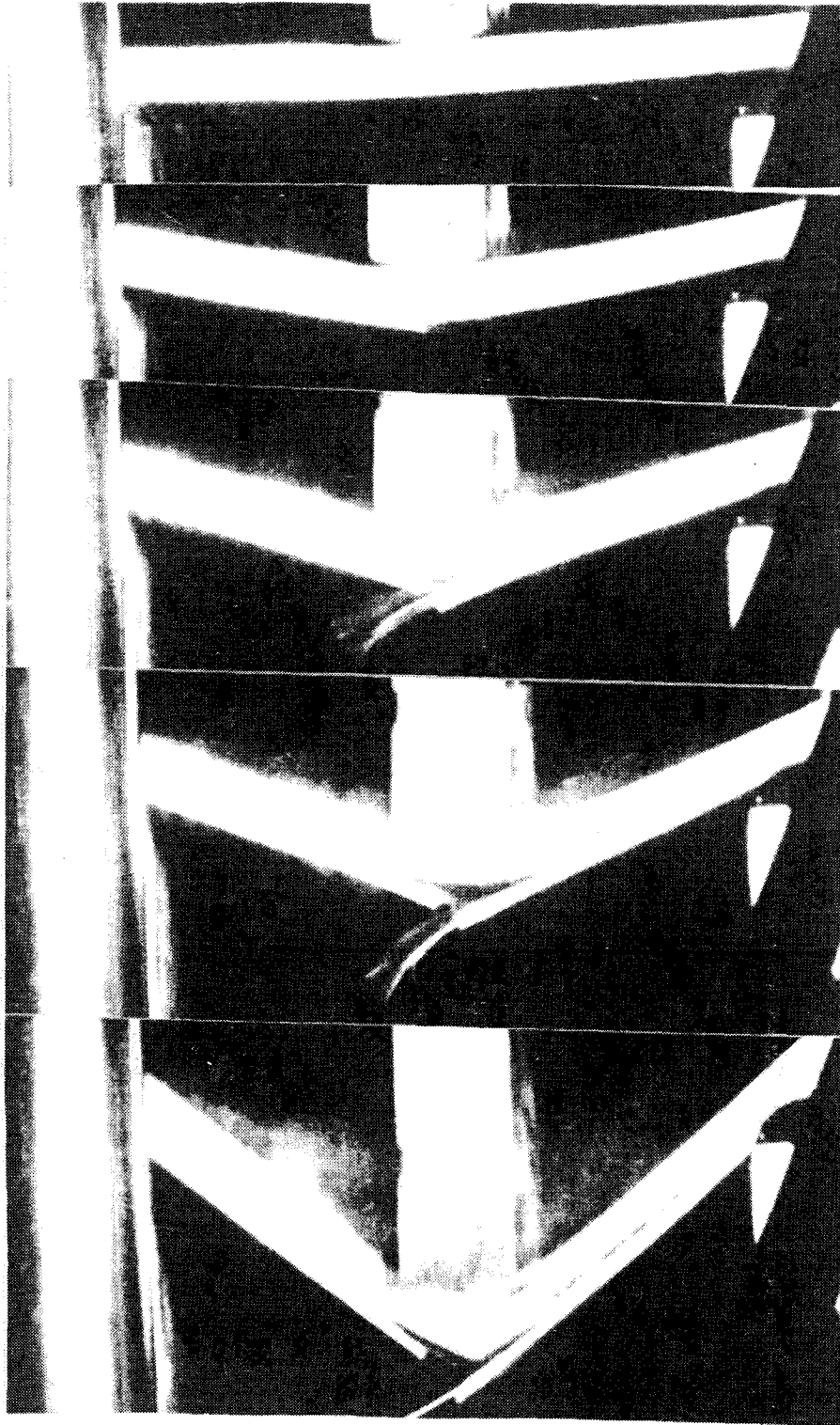


Figure 43. Impact sequence (LV3)
at time 0, 4, 6, 8, and 16 ms.

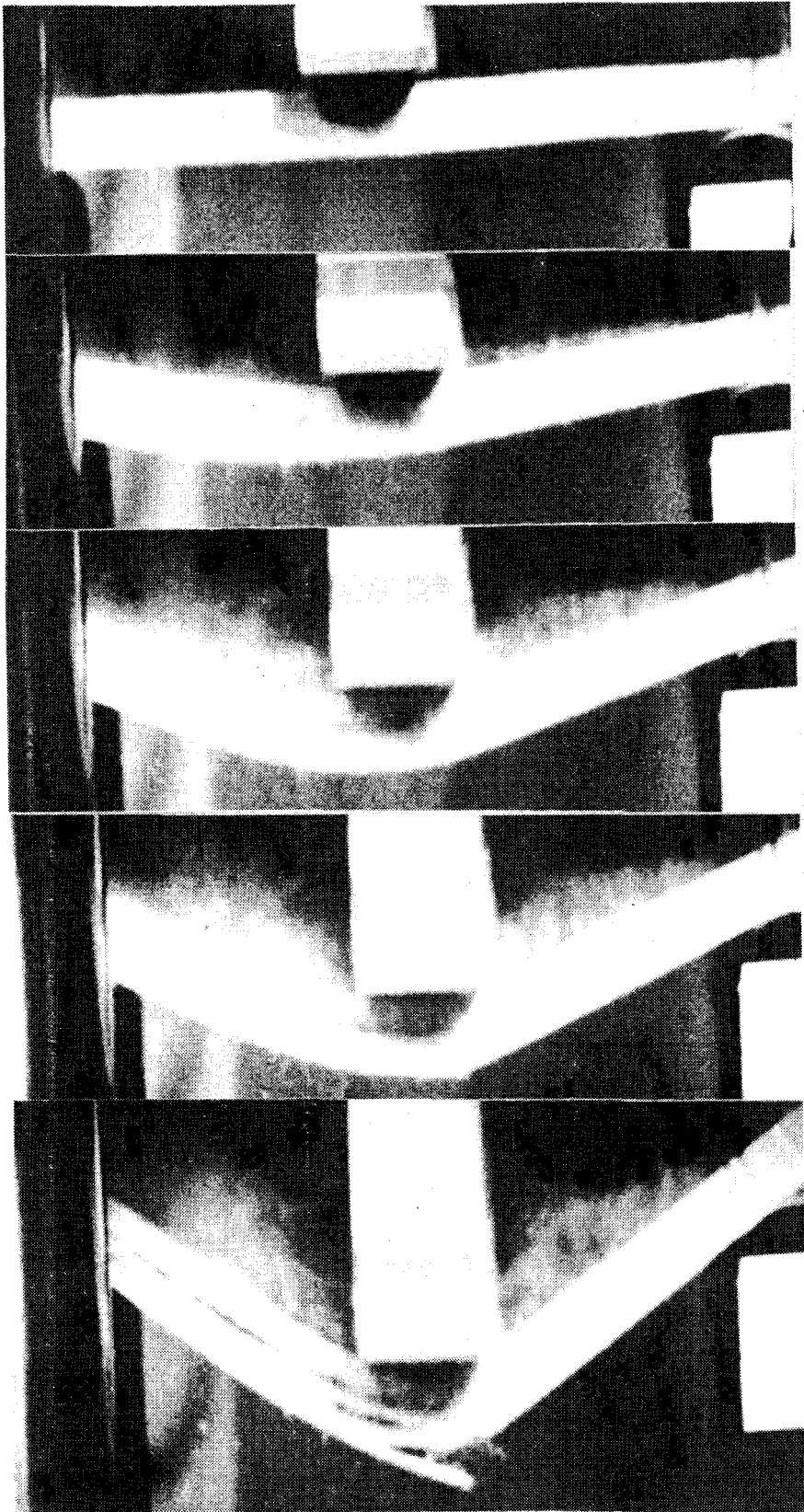


Figure 44. Impact sequence (LV4)
at time 0, 3, 7, 9, and 14 ms.

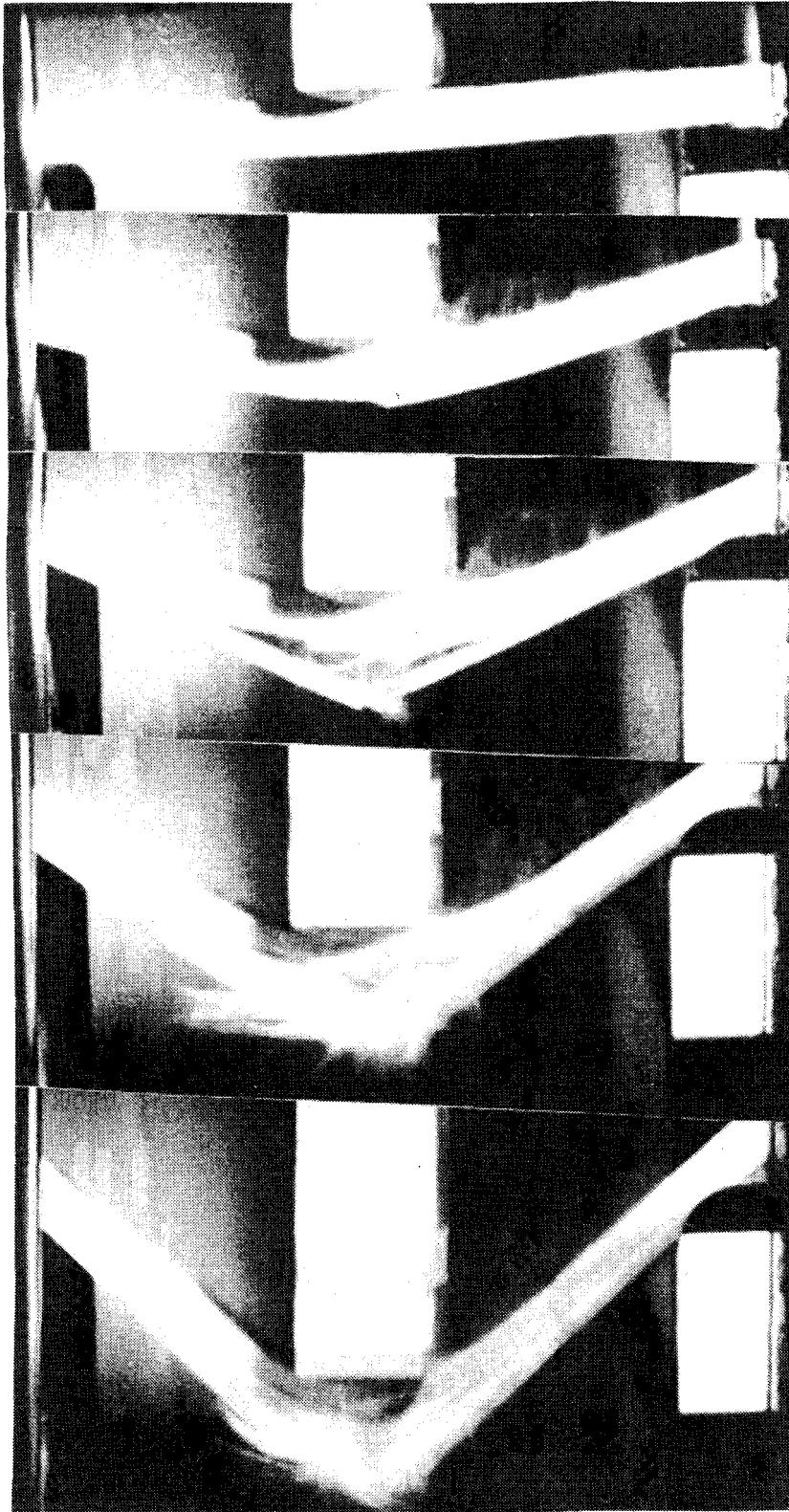


Figure 45. Impact sequence (LP3)
at time 0, 6, 8, 12, and 17 ms.

fiber specimens exhibited the first failure mechanism type. That is, they initially failed in tension from extreme fibers, then failed in shear due to delamination of the layers. In all of the photographic sequences previously described, the final photograph corresponds to the end of the impact event (i.e., the point in time when the velocity reaches its local minimum value).

CHAPTER 4. LABORATORY FABRICATION OF COMPOSITE MATERIALS

Test specimens were also fabricated by hand lay-up in a laboratory vacuum bag process for a second series of impact tests. This chapter describes the laboratory fabrication procedure used to fabricate the specimens for this series of impact tests. Unlike the automated pultrusion process, the hand lay-up procedure allows the use of a wider variety of fiber fabrics and ply orientations. This process, although suitable for the small-scale testing conducted in this study, is generally not practical for large-scale operations.

Fabrication Procedure

Figure 46 illustrates a cross section of a typical vacuum bag set-up. The lay-up, consisting of fiber plies, resin, and a release material or bleeder, is placed between two flat steel plates. The plates and lay-up are wrapped in a resin-absorbing layer of burlap to absorb and protect the vacuum pump from excess liquid resin. Then, this assembly is placed inside a vacuum bag that is sealed at all ends with an all-purpose sealant. When the vacuum pump is switched on, the lay-up is subjected to atmospheric pressure of up to 100 kPa (14.5 lbf/in²).⁽¹⁰⁾ The steel plates ensure that the composite remains flat during the curing process. The composite is cured in the vacuum bag until a solid cure is established, usually about 2 hours.

Test Specimens

Twenty different plates were fabricated using the hand lay-up laboratory procedure. They were composed of five types of fiber systems and four different matrix materials. Five fiber orientations and four resin types were considered. The fiber orientations consisted of a 0 rad (0°) to 1.57 rad (90°) cross-ply woven roving (C), 0 rad (0°) unidirectional (longitudinal) (L), 1.57 rad (90°) unidirectional (transverse) (T), ± 0.785 rad (45°) angle-ply stitched roving (F), and a chopped strand random mat (R). The resins consisted of two polyesters: Owens Corning E701 (E) and Ashland Aropol 2036 (A), and two vinyl esters: Ashland Hetron 922 (H) and Interplastics VEX168-586 (V). The letter in parentheses following each fiber and resin was used to denote the test specimen. For example, the cross-ply with the E701 polyester resin was denoted as CE. For each specimen type, three specimens were tested and were designated as 01, 02, and 03. All test specimens had a nominal width of 25 mm (1.0 in) and a nominal length of 178 mm (7.0 in). Table 3 presents the test specimen thicknesses for the laboratory-fabricated material.

Table 3. Average thickness - laboratory-fabricated material.

Thickness [mm (in)]

RESIN	FIBER SYSTEM				
	C	F	L	R	T
E	3.5 (0.14)	3.5 (0.14)	4.0 (0.16)	2.7 (0.11)	3.8 (0.15)
A	3.4 (0.13)	3.8 (0.15)	4.0 (0.16)	2.7 (0.11)	4.0 (0.16)
H	3.5 (0.14)	3.8 (0.15)	4.0 (0.16)	3.0 (0.12)	4.0 (0.16)
V	3.5 (0.14)	4.0 (0.16)	4.0 (0.16)	3.0 (0.12)	4.0 (0.16)
AVE	3.5 (0.14)	3.8 (0.15)	4.0 (0.16)	2.9 (0.11)	4.0 (0.16)

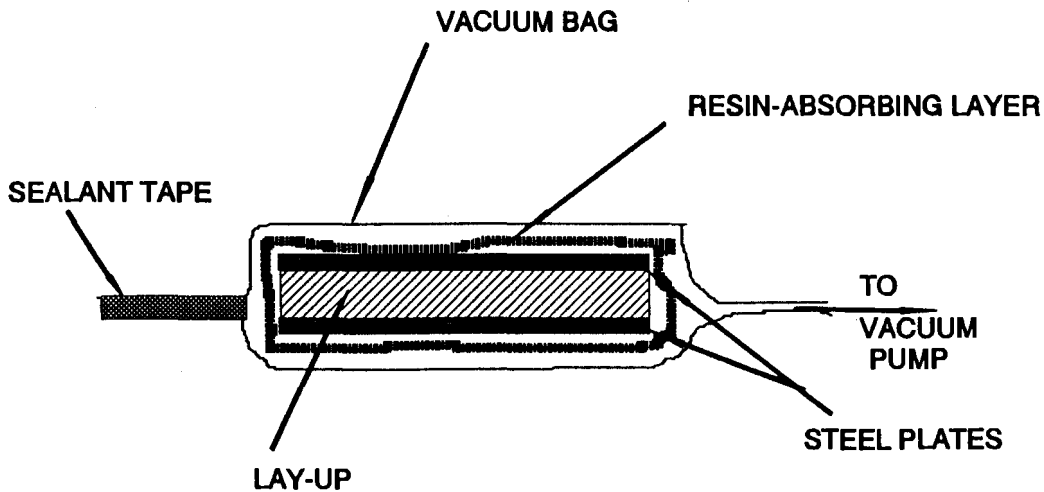


Figure 46. Laboratory fabrication.

CHAPTER 5. IMPACT TESTS ON LABORATORY-FABRICATED MATERIAL

Test Results

Impact test conditions for the laboratory-fabricated material specimens are the same as for the pultruded material. When tested, only longitudinally (L) and cross-ply-reinforced (C) specimens had a failure strength that could be detected by the instrumented data acquisition system. All other specimen types, with the exception of the angle-ply (F), were weak and failed at a load level that was too low to be detected. The angle-ply (F) specimens did not fail when impacted. These specimens were flexible and deflected out of the path of the striker with little or no apparent external damage. Plots of the load versus time curves grouped according to specimen type are presented in figures 47 through 54 [for (L) and (C) specimen types]. The corresponding energy versus time curves are shown in figures 55 through 62. As before, averaging each point in time from the load versus time and the energy versus time curves produces a single average curve for each specimen type. Figures 63 through 70 show the average load versus time curves and figures 71 through 78 show the average energy versus time curves. Also, the average load plus and minus one standard deviation is plotted as figures 79 through 86. Again, the average load has been omitted from the standard deviation plot for clarity.

In order to compare results from these tests to the pultruded material described previously, the results have been normalized by all geometric parameters in the same manner. The normalized load values are presented in figure 87. The normalized energy values are presented in figure 88. Comparing figure 87 with figure 41, it can be seen that the cross-ply (CE, CA, CH, and CV) specimens carry comparable amounts of load with the primarily longitudinal pultruded material (LV2, LV3, and LP3). The longitudinal (LE, LA, LH, and LV) specimens, on the other hand, carry 0.5 to 2.5 times more load than the primarily longitudinal pultruded specimens. Comparing figure 88 with figure 42, it is apparent that the cross-ply specimens absorb energy comparable to the primarily longitudinal pultruded material, while the longitudinal specimens absorb 2 to 5 times more energy than the primarily longitudinal pultruded. The average load and energy values taken from the average curves are presented in table 4 for the important data analysis points.

Comparison with Pultruded Material

In many ways, the laboratory-fabricated material shows the same characteristics as the pultruded material tested on the load versus time curves. The polyester resin specimens (resin designation E or A) all have an initial nearly linear elastic part of the curve until the initiation load. Then, a region of tensile fiber failures exists until the load value drops off to zero. This compares to the characteristics of the LP3 curve from the pultruded material. This can be seen by comparing the average curves in figures 67 and 68 with figure 21. Also, the vinyl ester specimens show some similarities in curve characteristics. Comparing figures 69 and 70 with figures 18 through 20, it is noted that both sets of curves have a sharp spike near the end of the impact event. This can be attributed to the predominance of a catastrophic shear failure in the material. This type of failure occurs

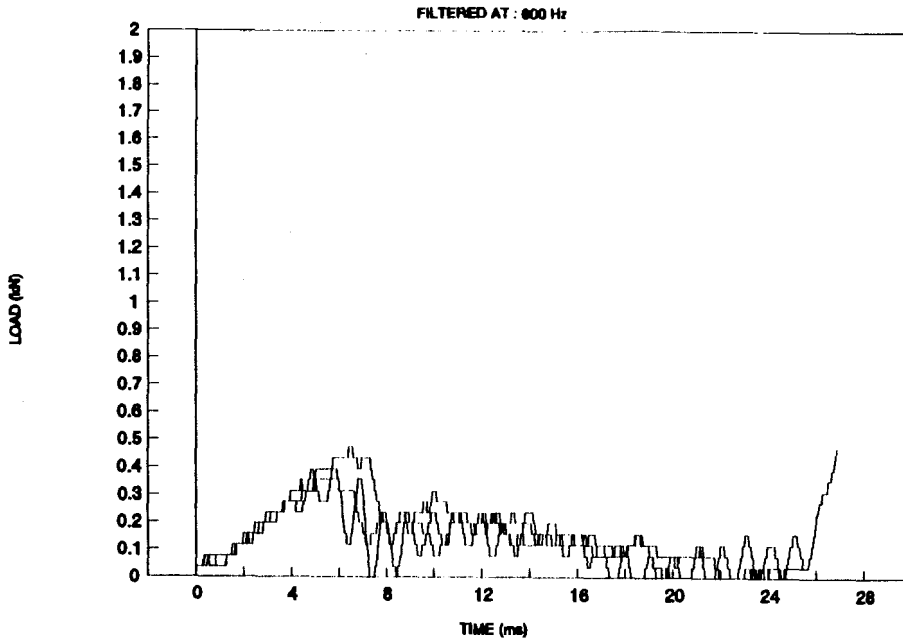


Figure 47. Load versus time (CE).

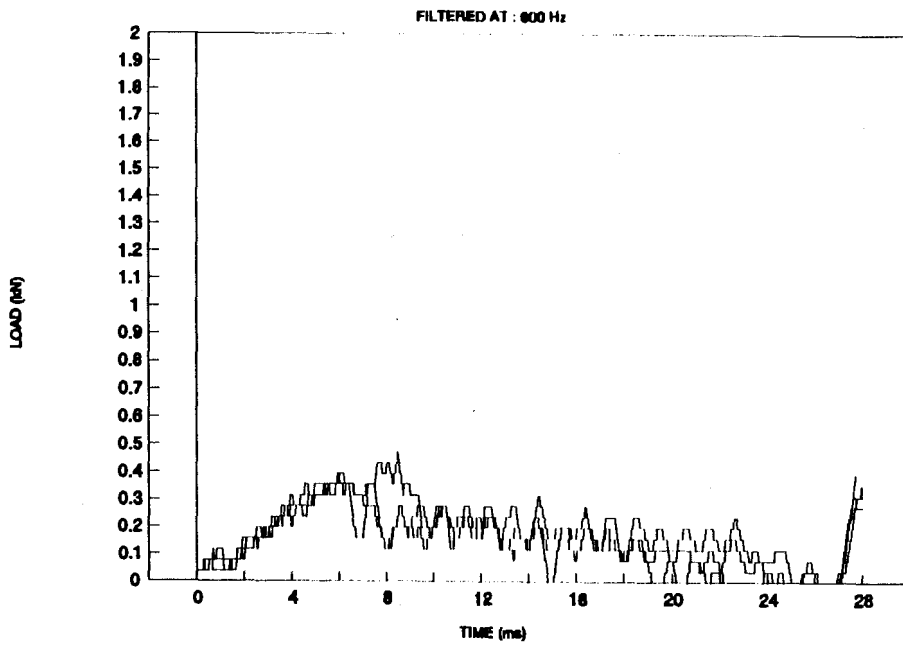


Figure 48. Load versus time (CA).

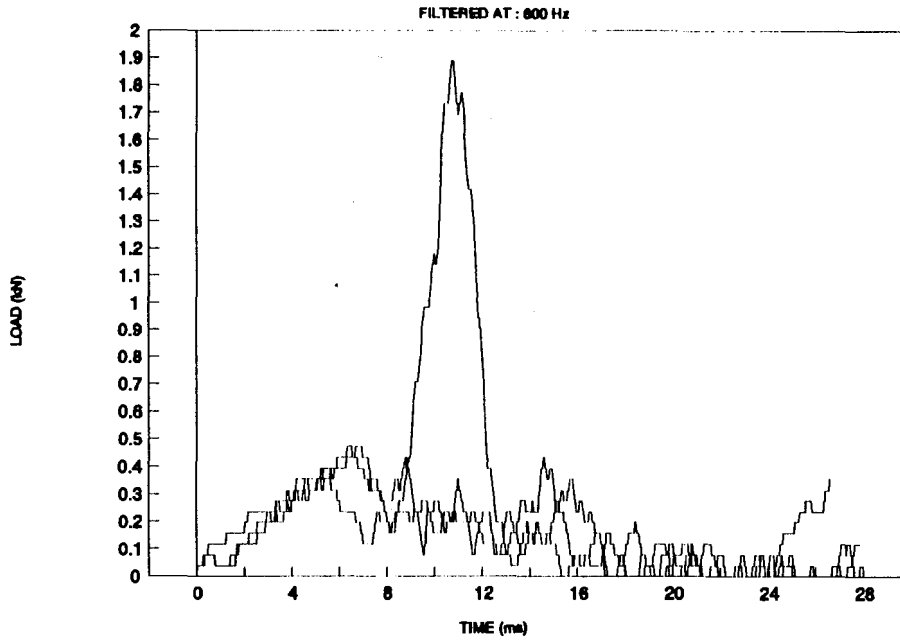


Figure 49. Load versus time (CH).

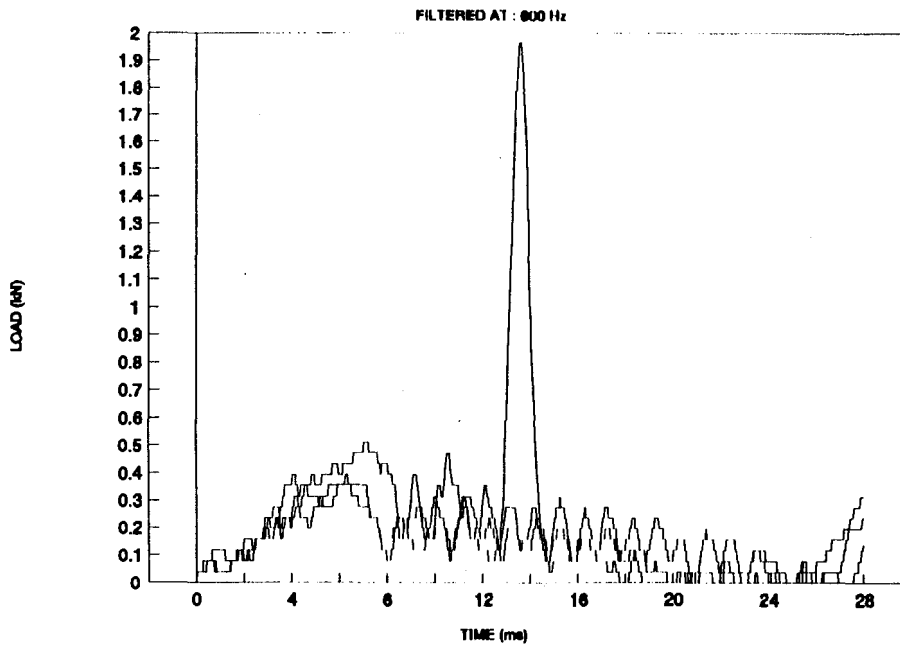


Figure 50. Load versus time (CV).

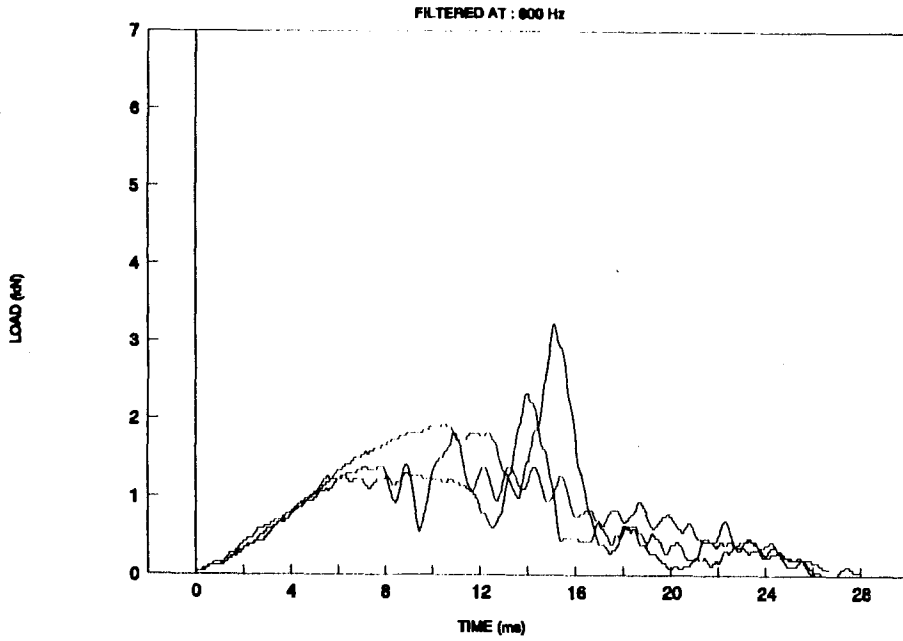


Figure 51. Load versus time (LE).

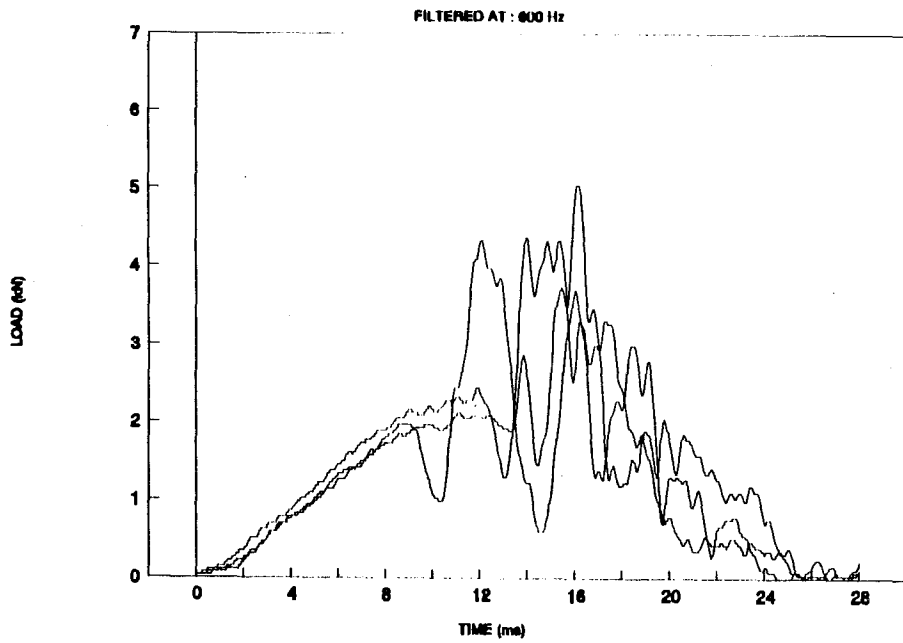


Figure 52. Load versus time (LA).

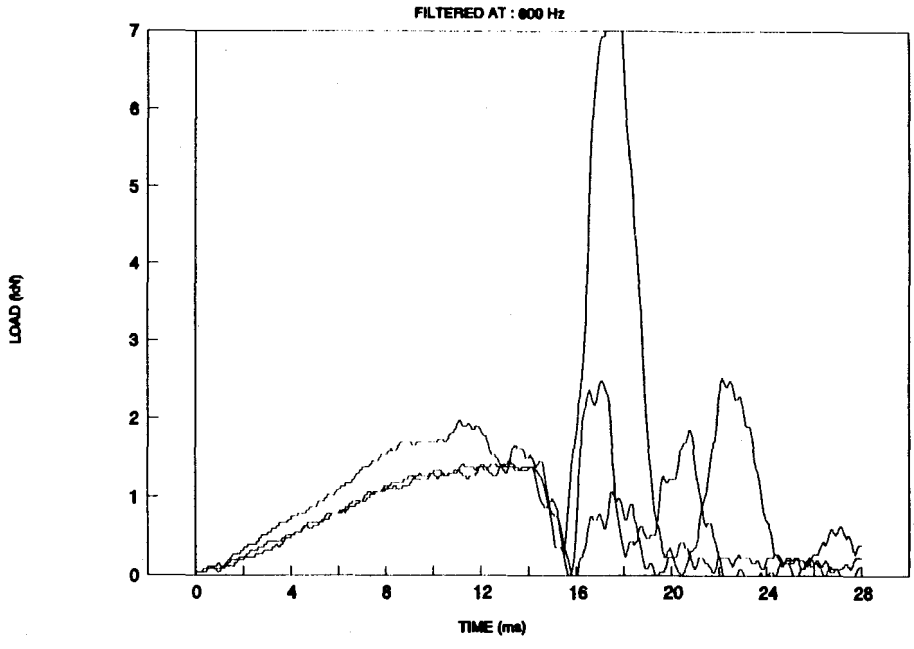


Figure 53. Load versus time (LH).

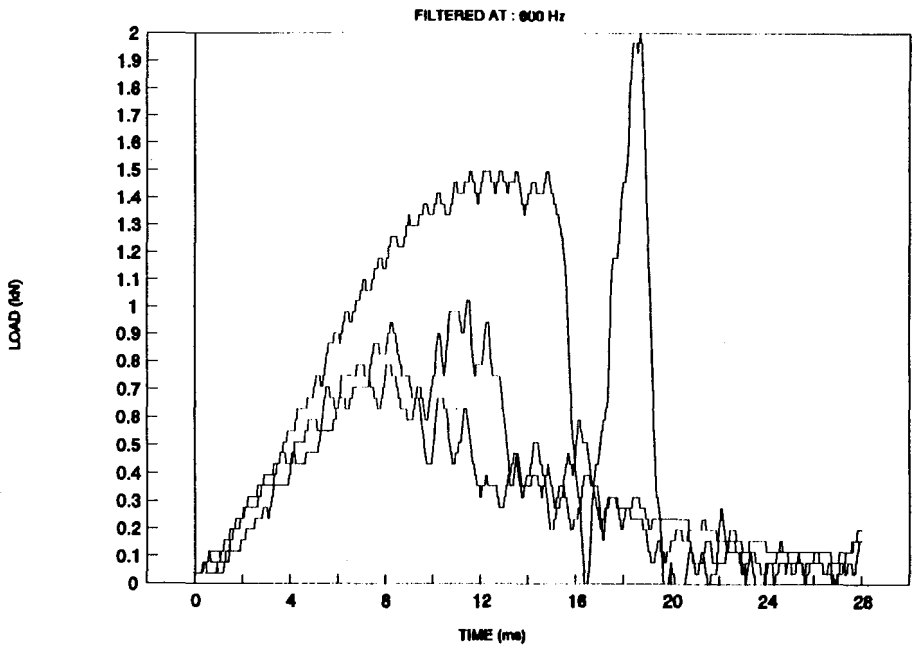


Figure 54. Load versus time (LV).

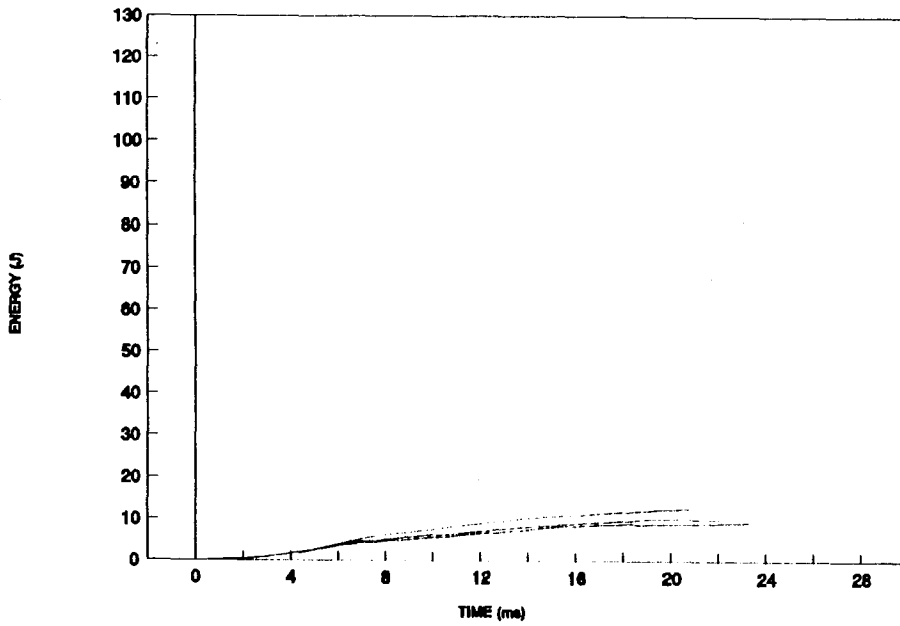


Figure 55. Energy versus time (CE).

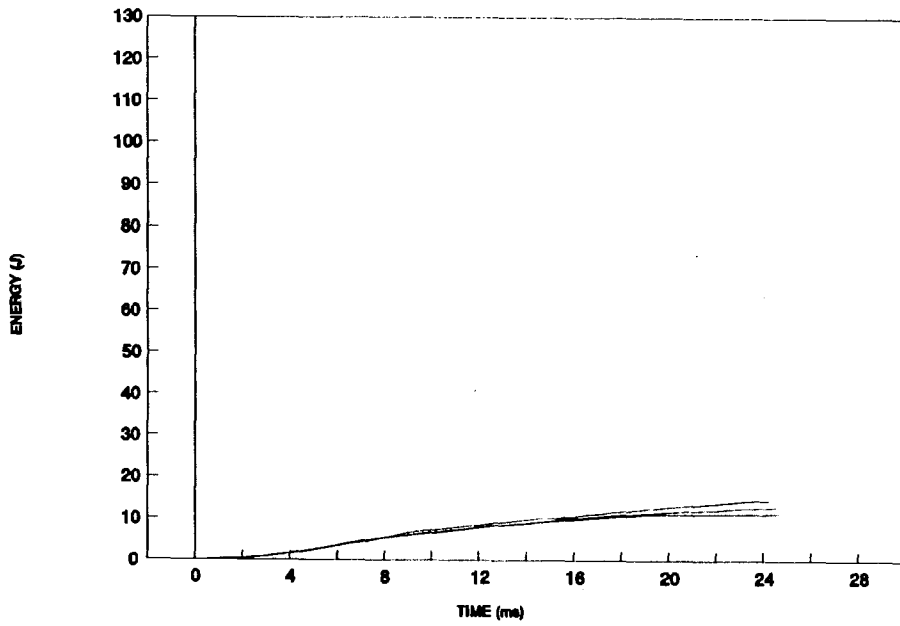


Figure 56. Energy versus time (CA).

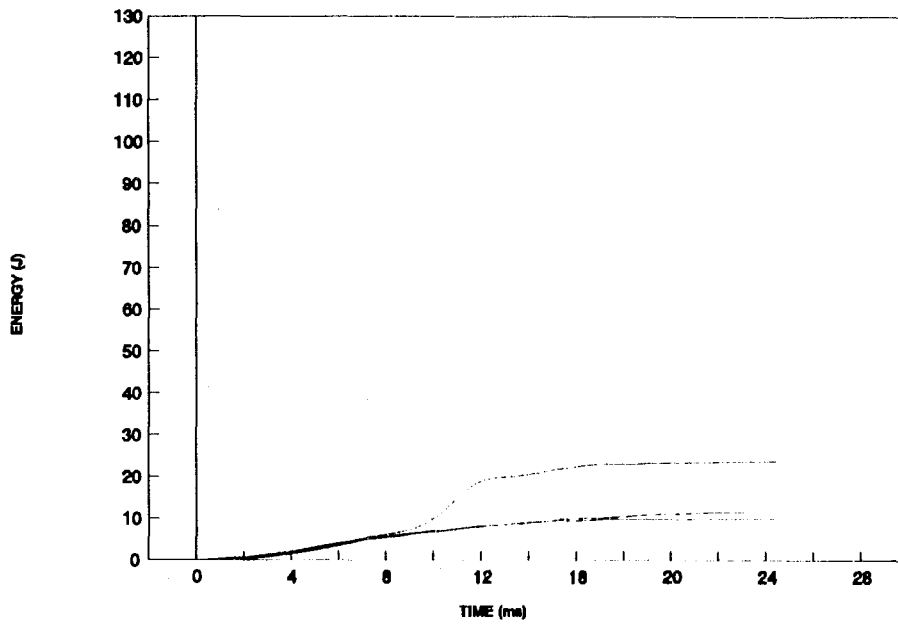


Figure 57. Energy versus time (CH).

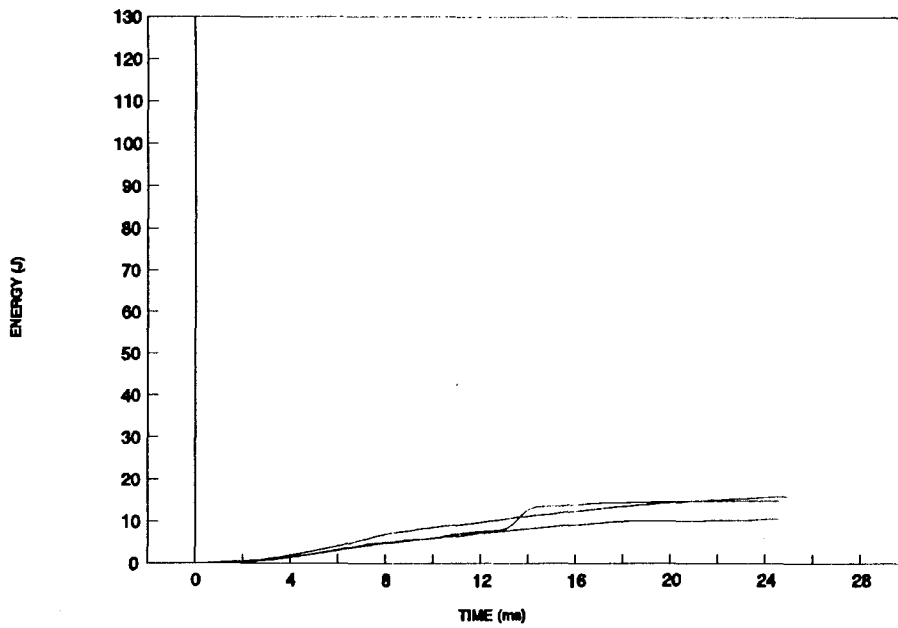


Figure 58. Energy versus time (CV).

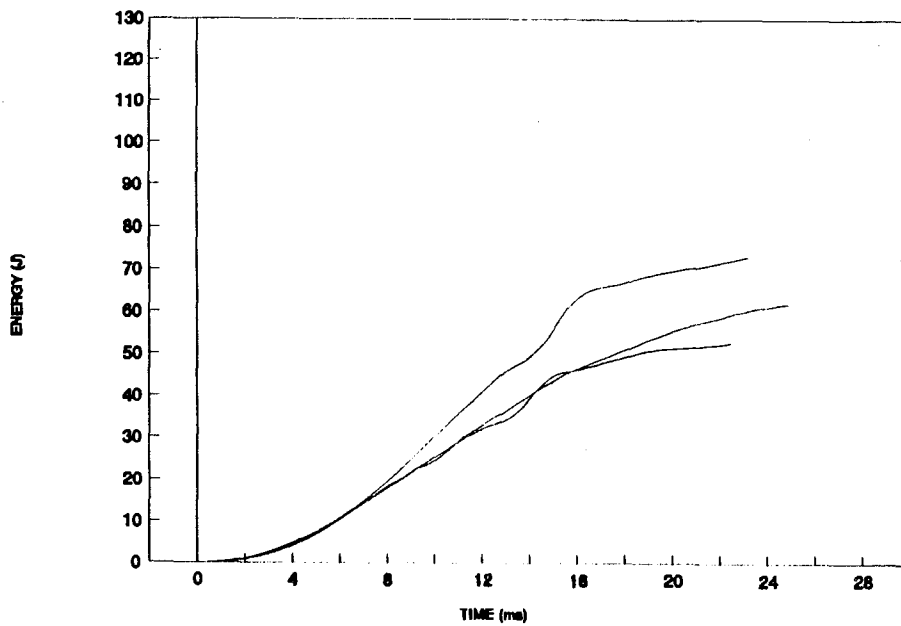


Figure 59. Energy versus time (LE).

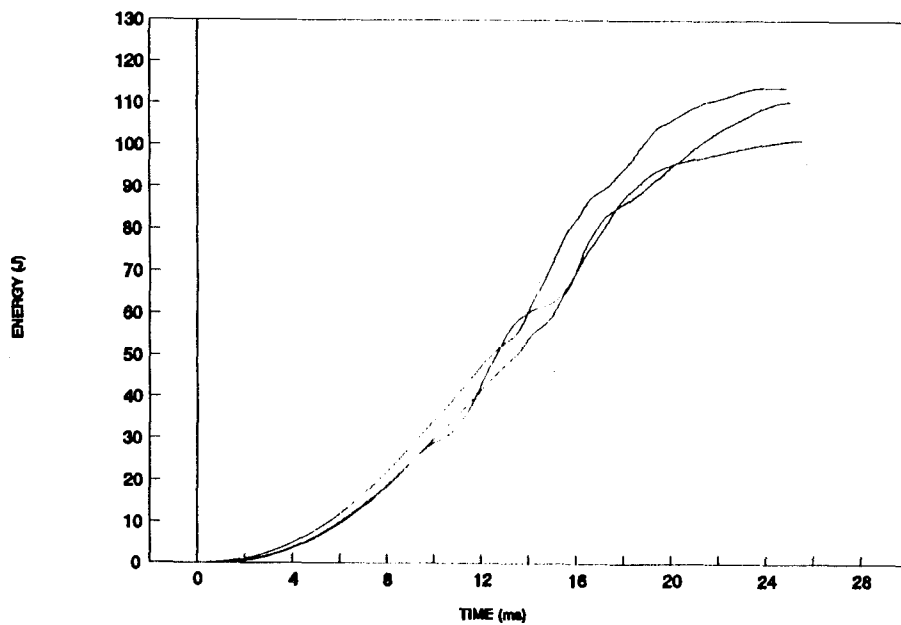


Figure 60. Energy versus time (LA).

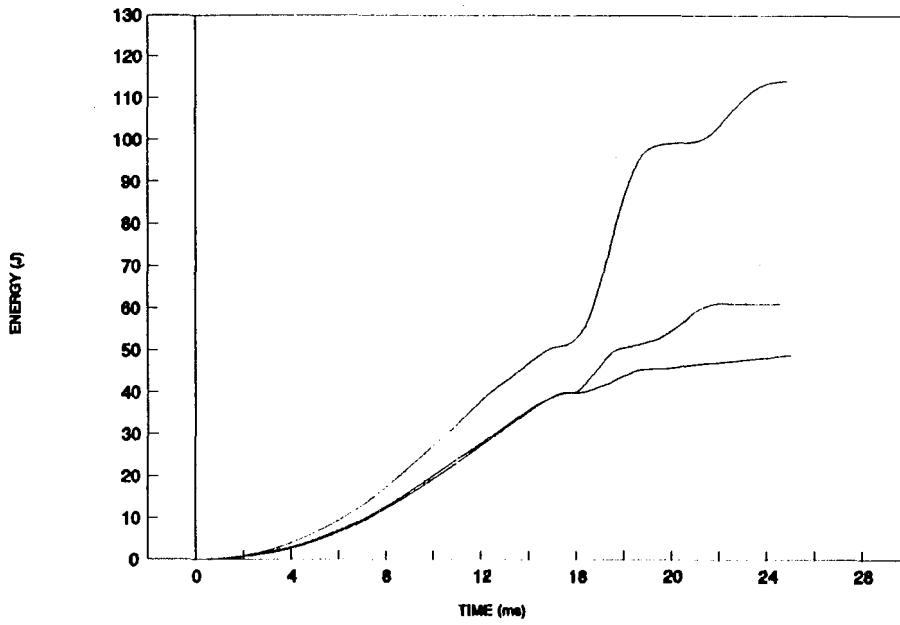


Figure 61. Energy versus time (LH).

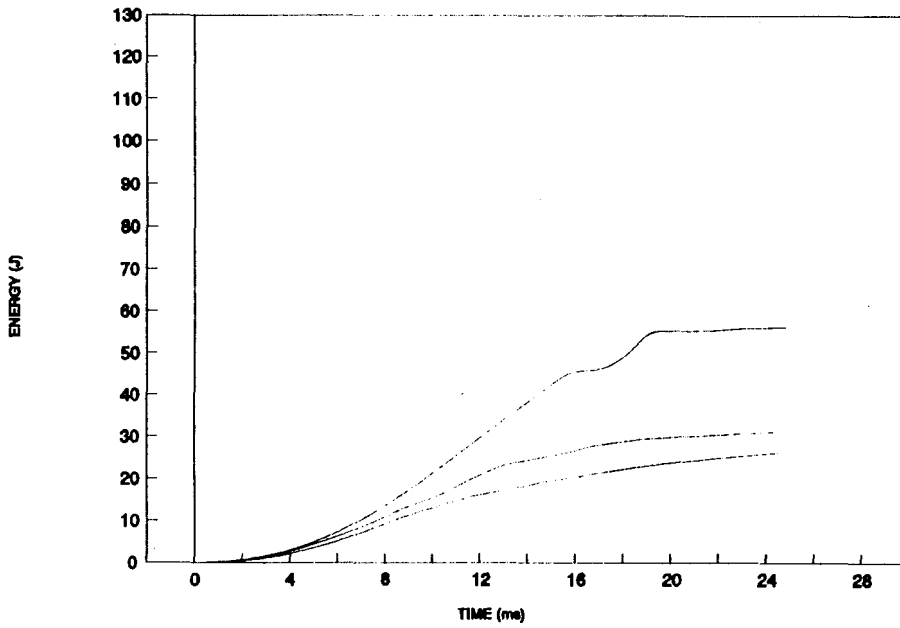


Figure 62. Energy versus time (LV).

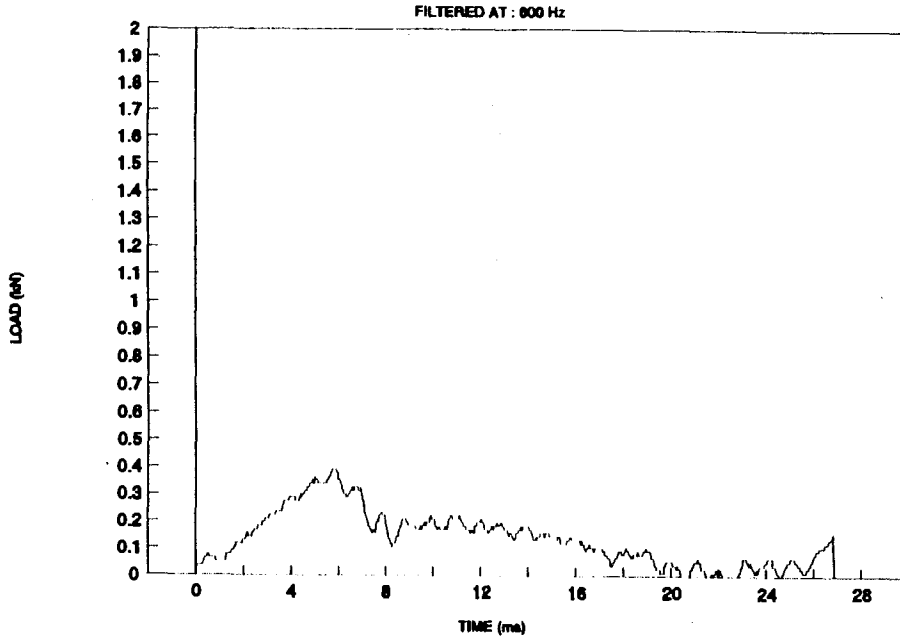


Figure 63. Average load versus time (CE).

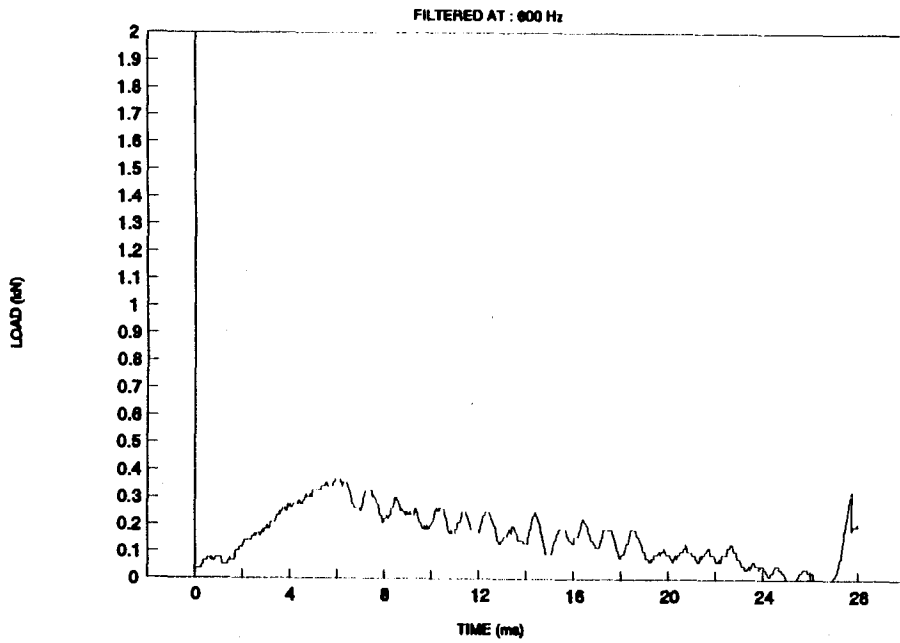


Figure 64. Average load versus time (CA).

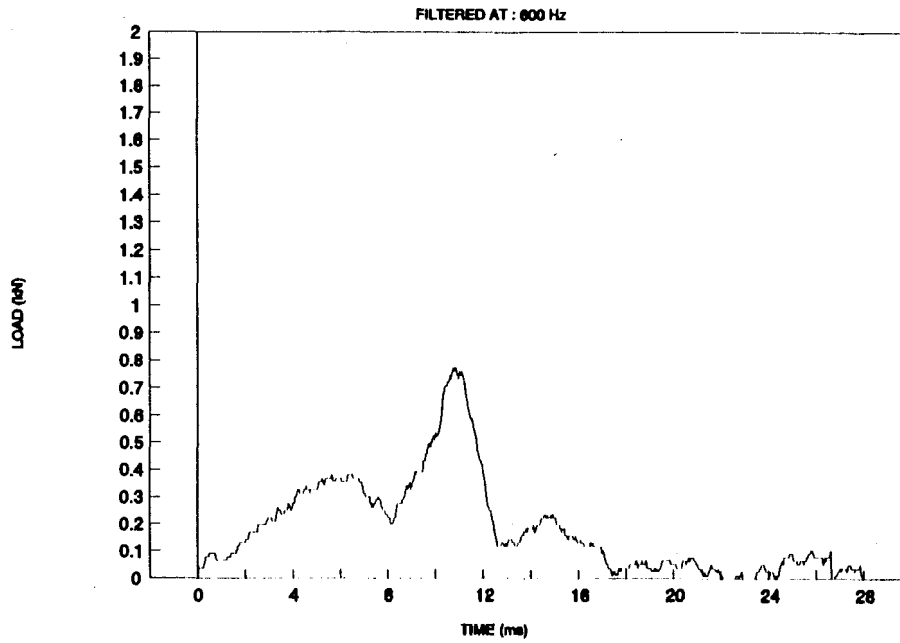


Figure 65. Average load versus time (CH).

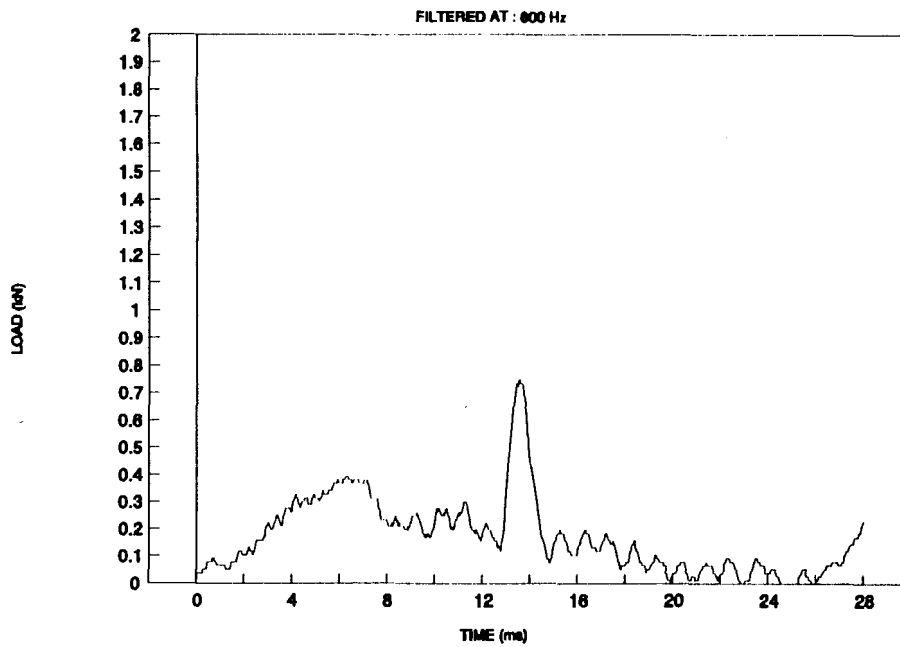


Figure 66. Average load versus time (CV).

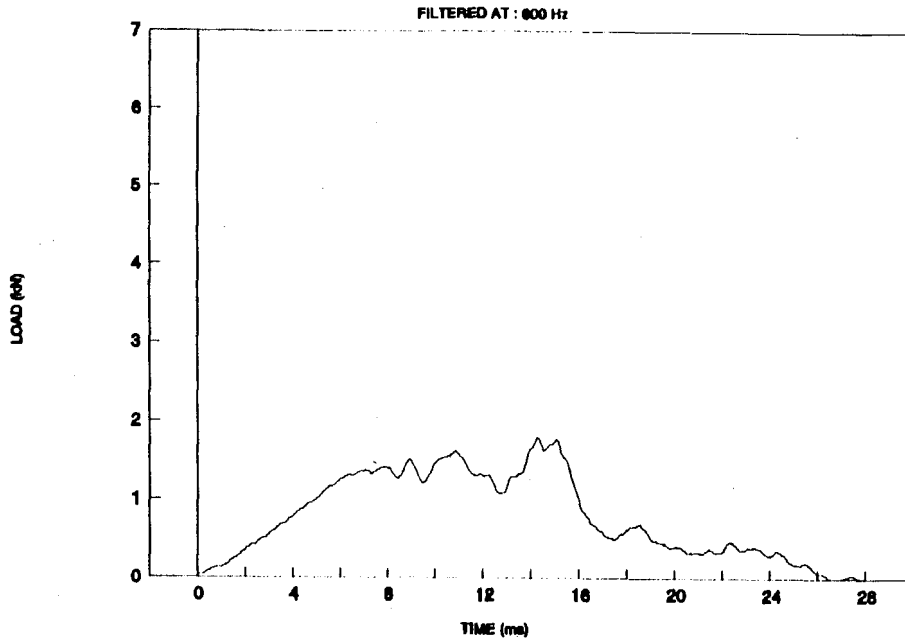


Figure 67. Average load versus time (LE).

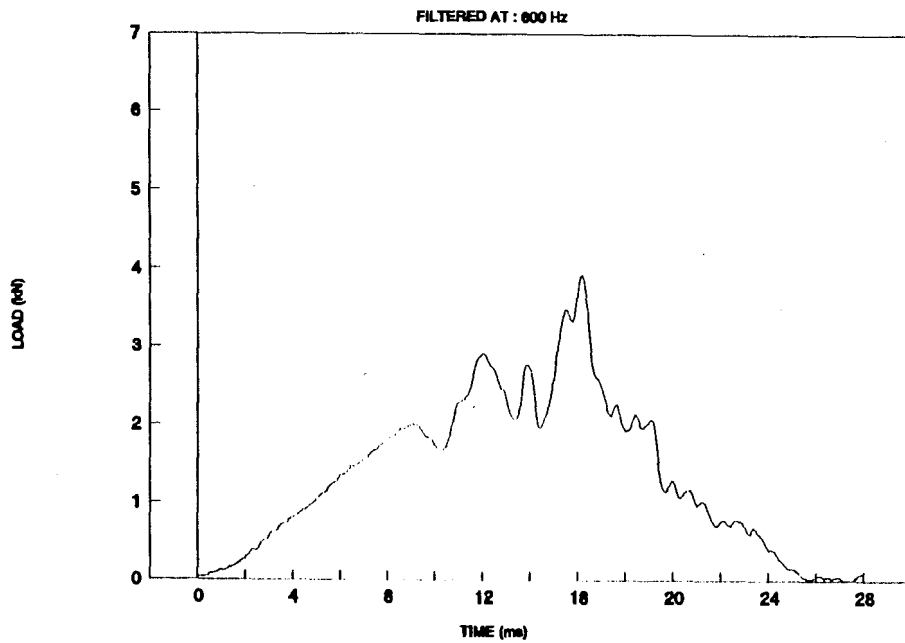


Figure 68. Average load versus time (LA).

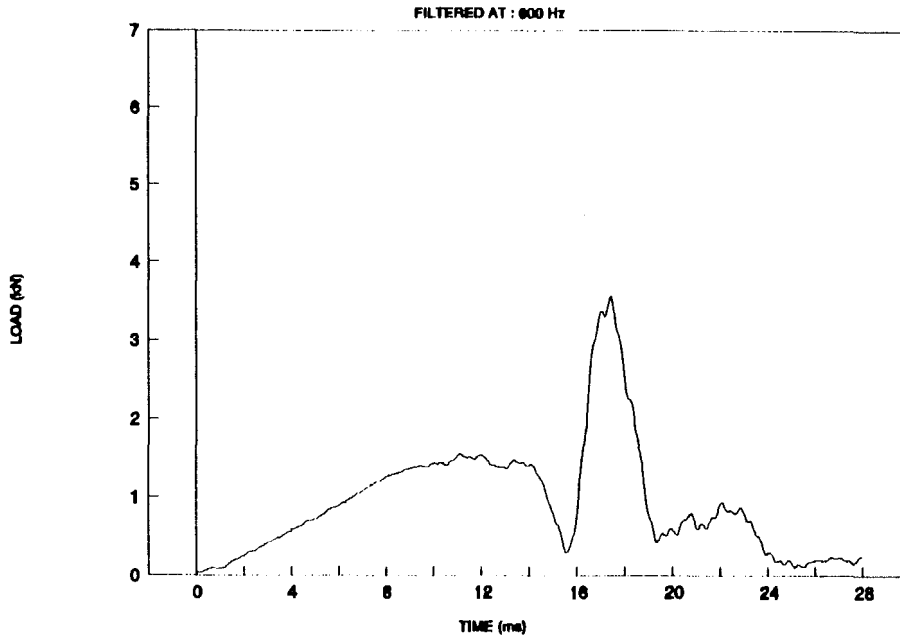


Figure 69. Average load versus time (LH).

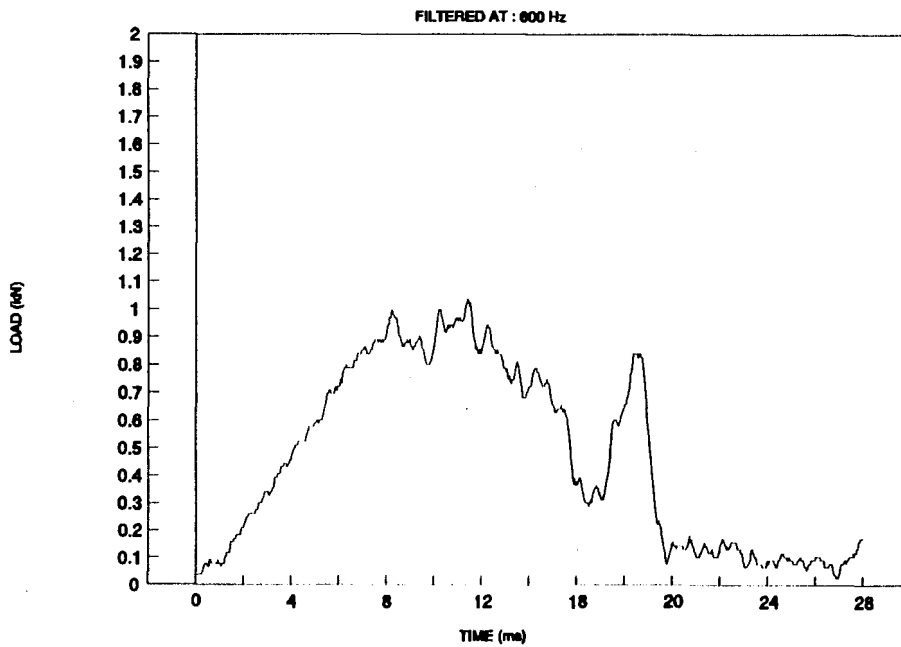


Figure 70. Average load versus time (LV).

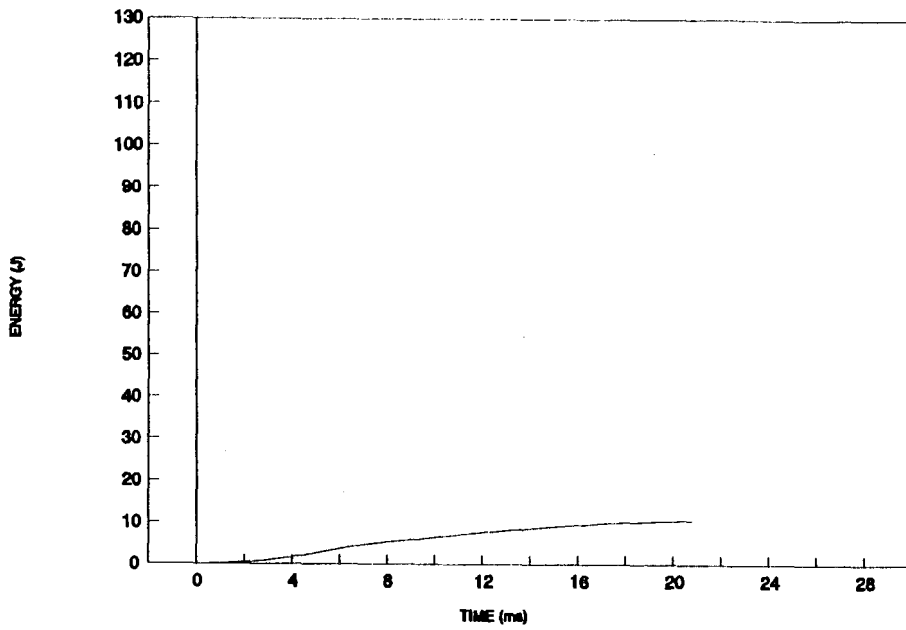


Figure 71. Average energy versus time (CE).

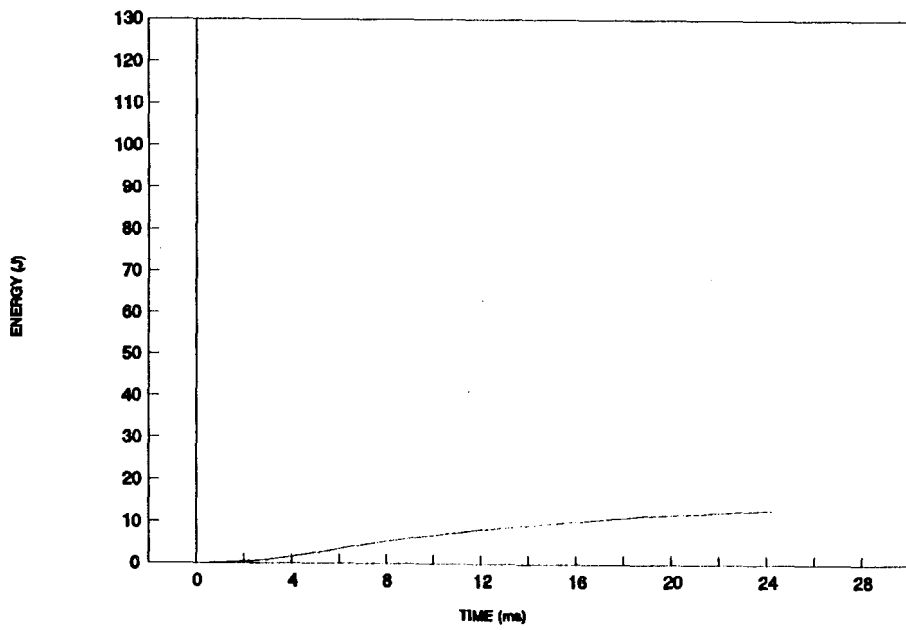


Figure 72. Average energy versus time (CA).

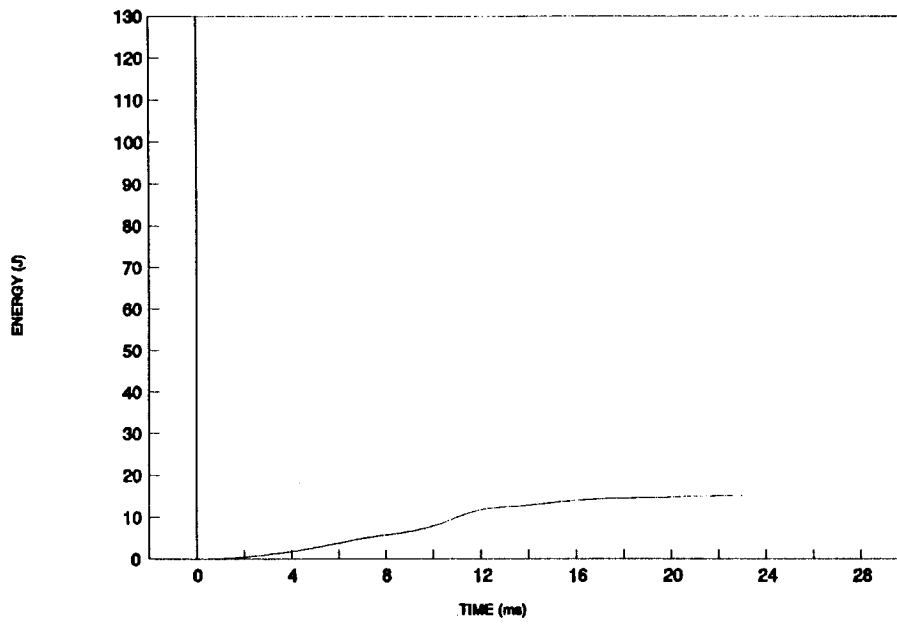


Figure 73. Average energy versus time (CH).

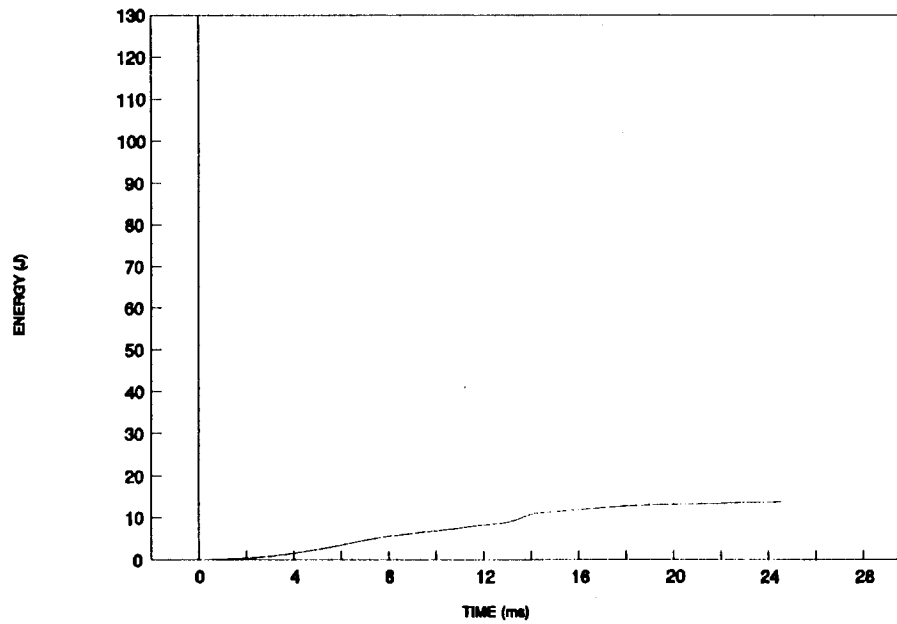


Figure 74. Average energy versus time (CV).

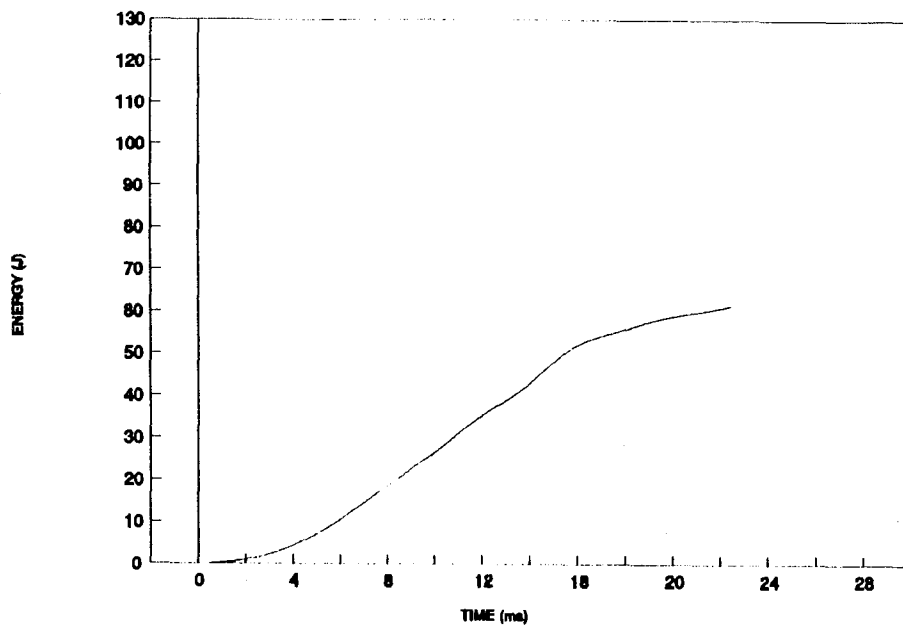


Figure 75. Average energy versus time (LE).

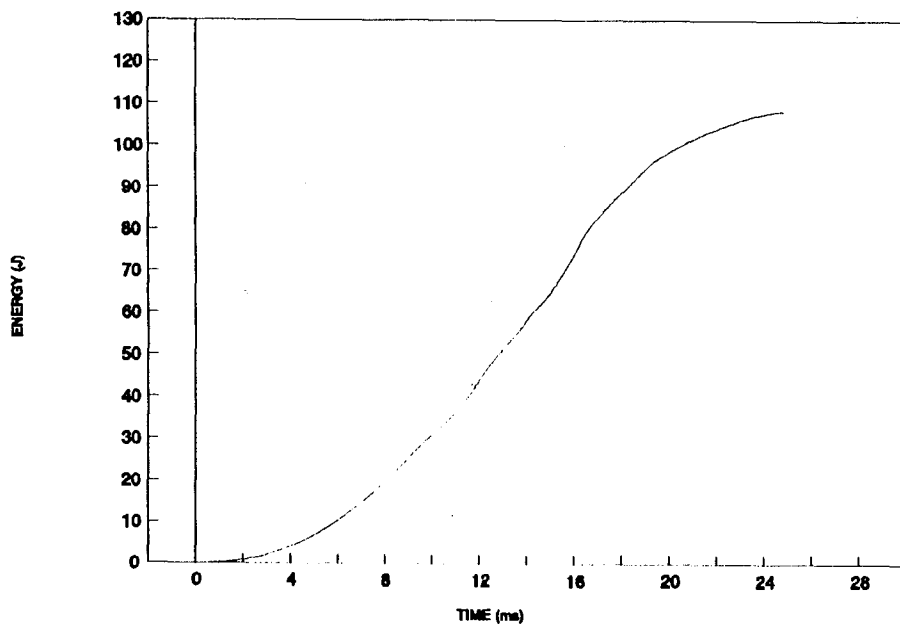


Figure 76. Average energy versus time (LA).

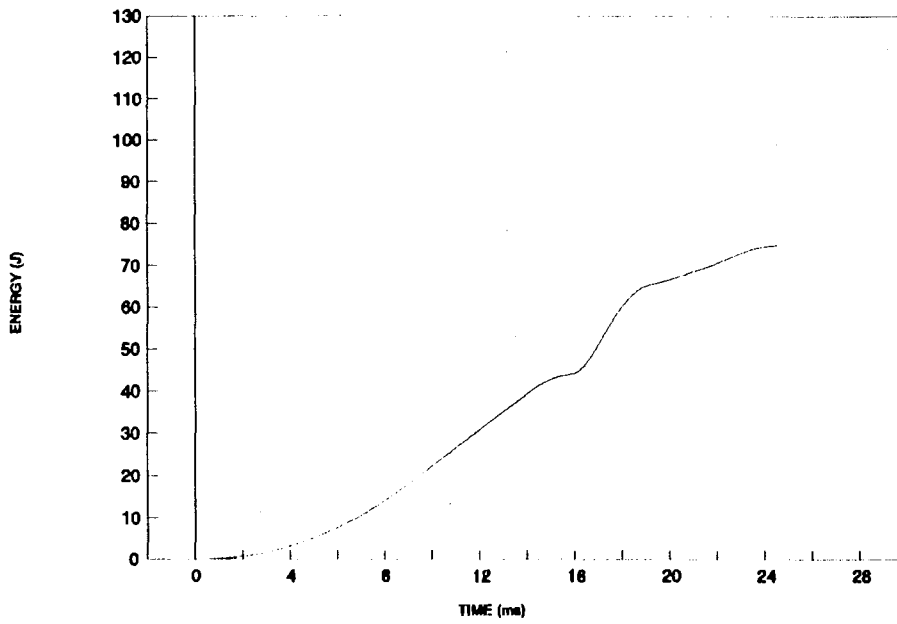


Figure 77. Average energy versus time (LH).

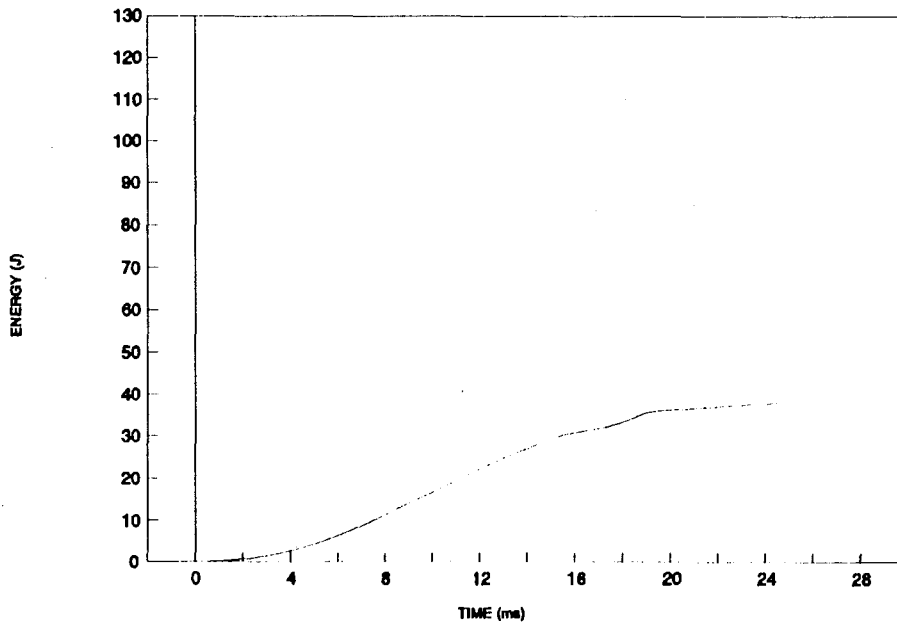


Figure 78. Average energy versus time (LV).

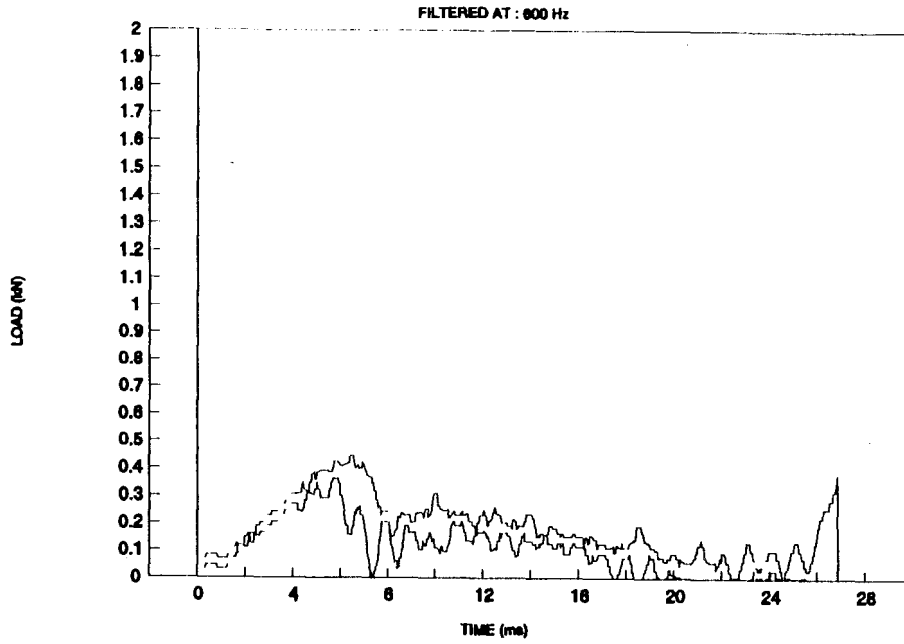


Figure 79. Standard deviation (CE).

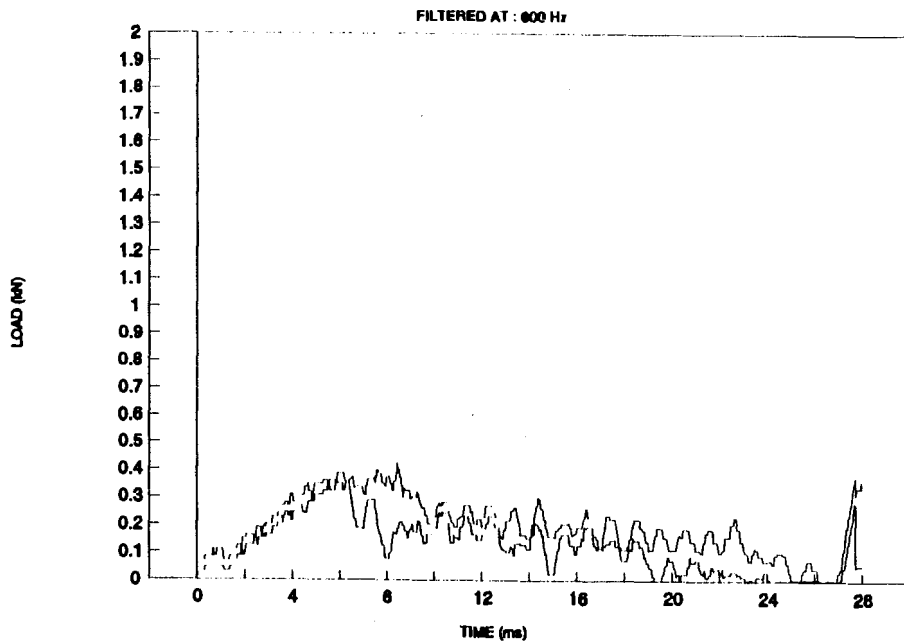


Figure 80. Standard deviation (CA).

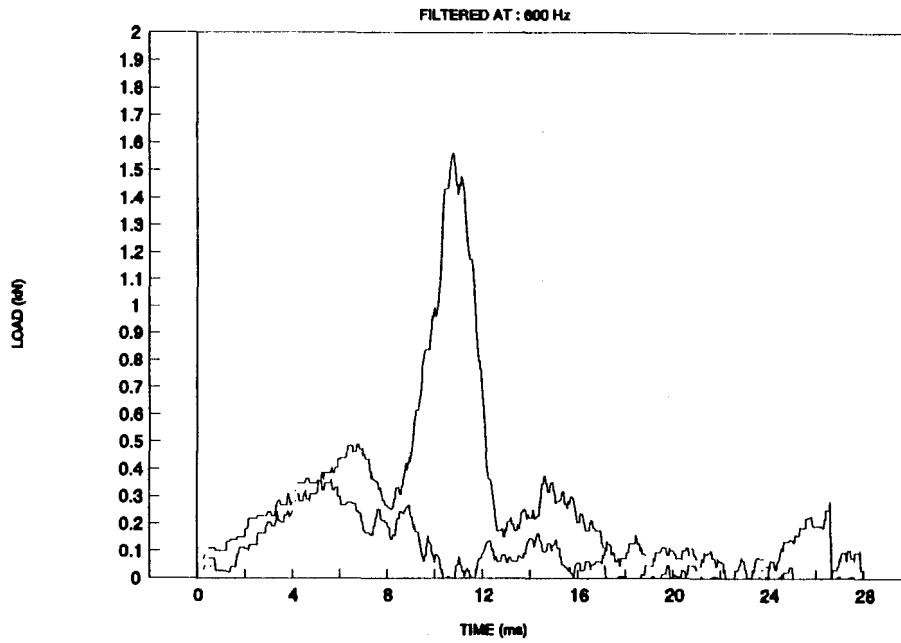


Figure 81. Standard deviation (CH).

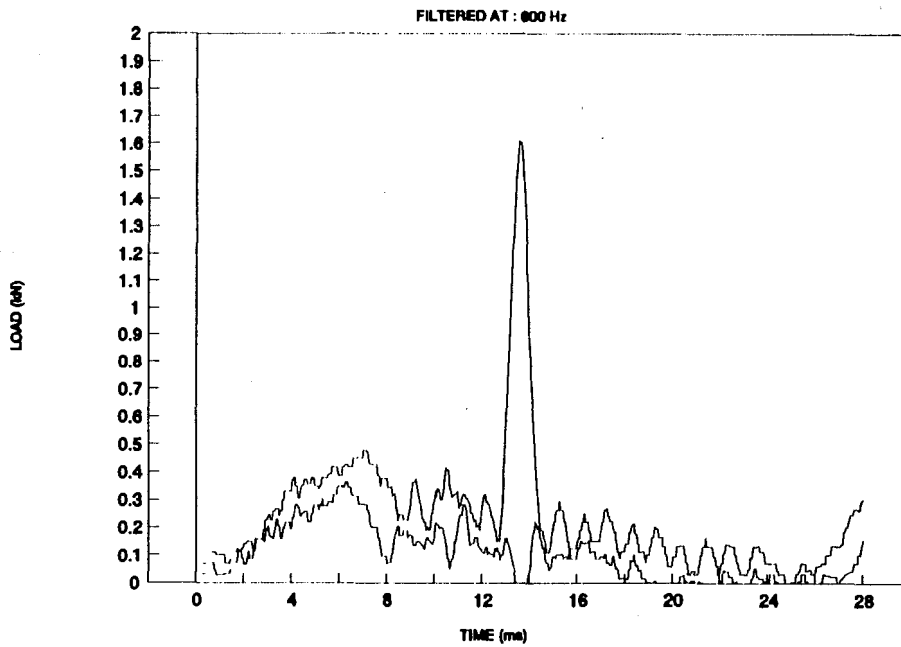


Figure 82. Standard deviation (CV).

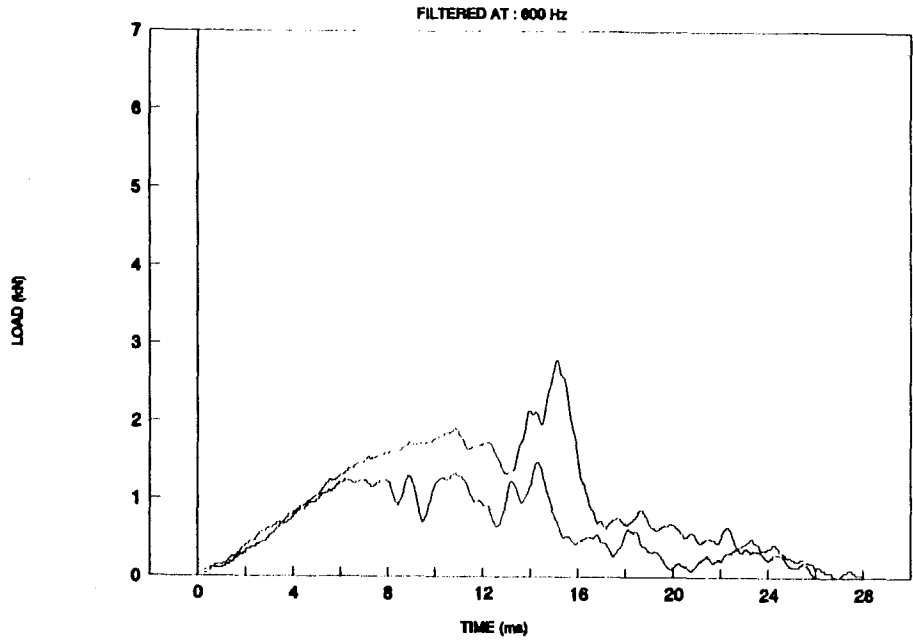


Figure 83. Standard deviation (LE).

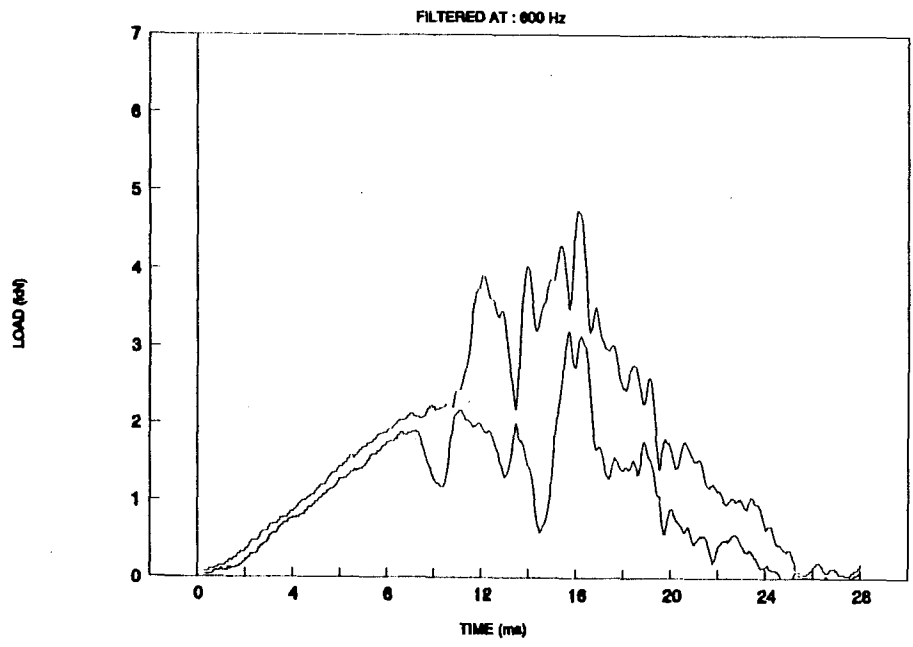


Figure 84. Standard deviation (LA).

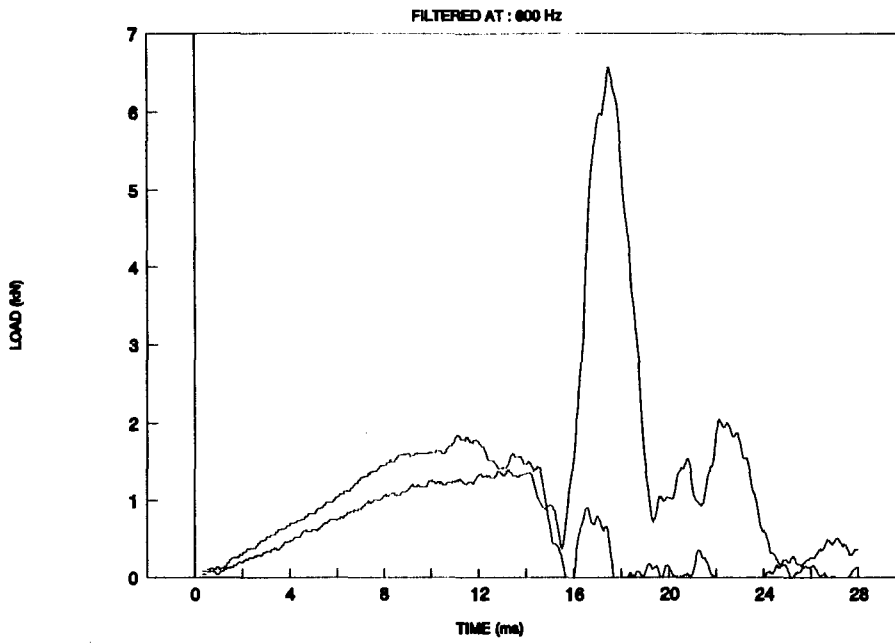


Figure 85. Standard deviation (LH).

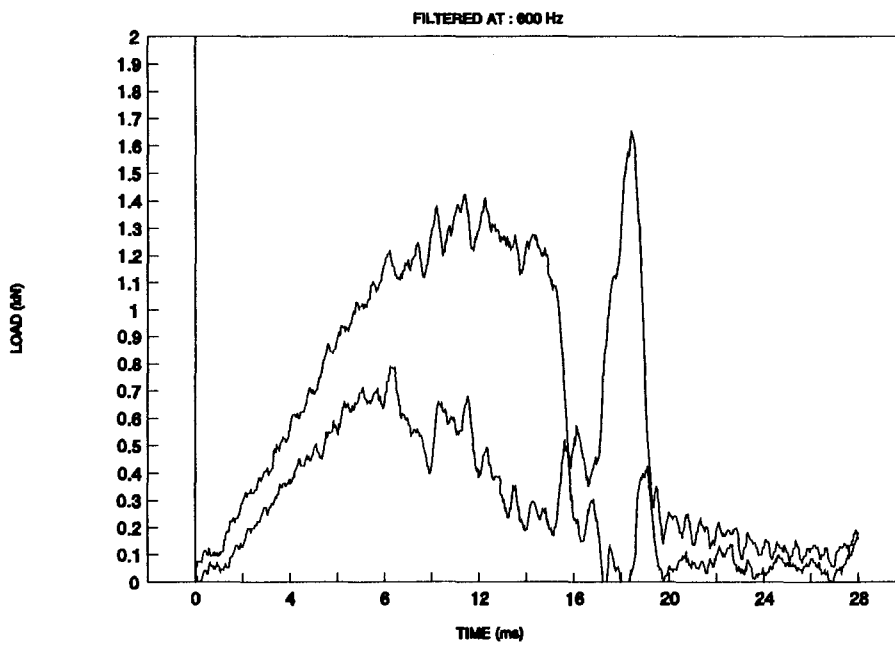


Figure 86. Standard deviation (LV).

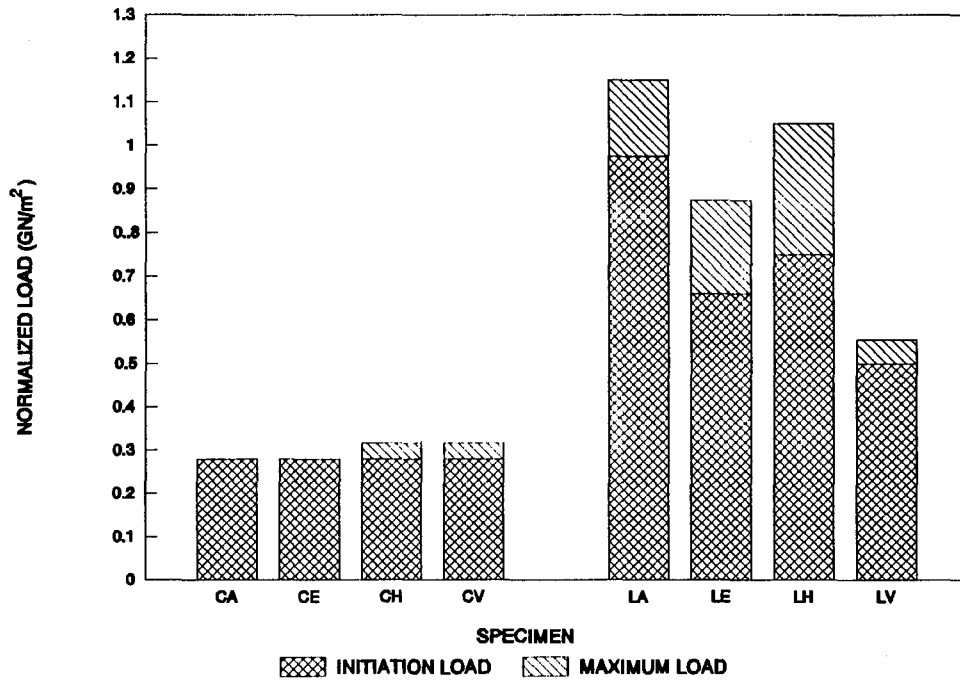


Figure 87. Normalized load - laboratory fabricated.

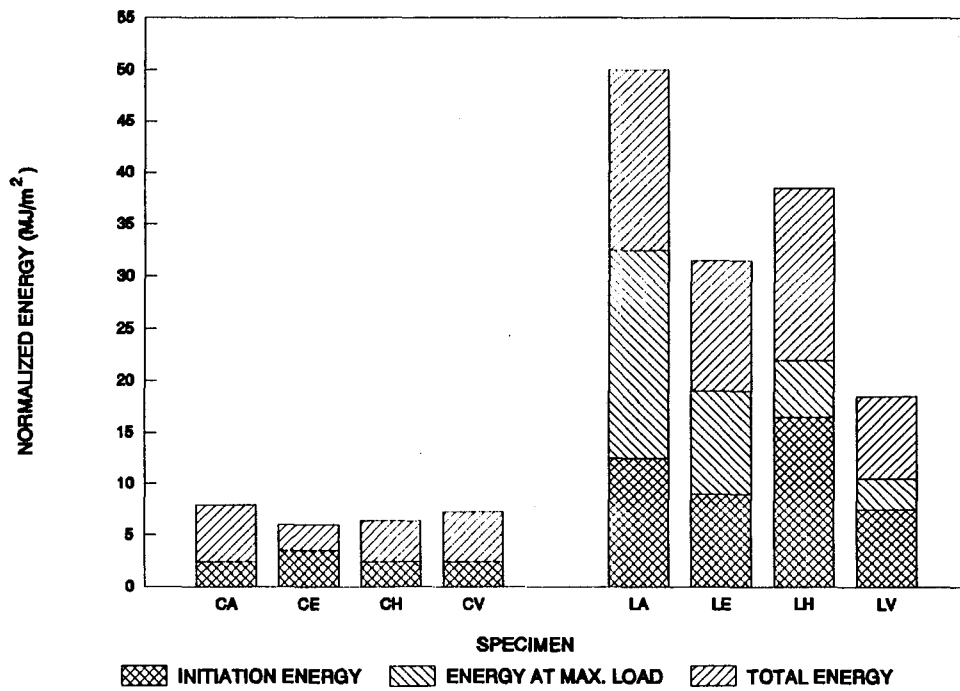


Figure 88. Normalized energy - laboratory fabricated.

Table 4. Average values - laboratory-fabricated material.

SPECIMEN	CA	CE	CH	CV	LA	LE	LH	LV
P_I , N	440	422	450	400	2010	1250	1226	1005
1b	98	95	101	90	452	281	276	226
E_I , J	4.8	4.8	4.7	5.8	33	28	23	17
ft-1b	3.6	3.6	3.5	4.3	25	21	17	13
P_M , N	442	422	815	780	2010	2011	4000	1150
1b	99	95	183	175	452	452	899	258
E_M , J	4.8	4.8	8.7	5.8	67	42	39	29
ft-1b	3.6	3.6	6.5	4.3	50	31	29	22
E_T , J	13	15	16	12	108	68	72	41
ft-1b	10	11	12	8.9	80	51	54	30

to some degree in all of the vinyl ester specimens tested, both pultruded and laboratory fabricated. The laboratory-fabricated material though, has a larger region of tensile fiber failures between the initiation load and the abrupt shear failure at the end.

Comparing the normalized energy (by all geometric parameters) results in figure 88 with the pultruded results in figure 42, it is apparent that the polyester specimens of both types have a large tensile failure region (represented by the center area of the bar). This is desirable as this is the area where there is the greatest amount of usable energy absorption in the material. In vinyl ester specimens, on the other hand, this region of energy absorption is small or absent completely. This is attributed to the catastrophic failure present in the vinyl ester specimens. The catastrophic failure of vinyl ester specimens could be due to the fact that in general, a vinyl ester matrix has a higher strain to failure than a polyester matrix. That is, the matrix material carries the load along with the glass reinforcement longer and the two fail in unison. The polyester composite, on the other hand, develops cracks early and allows for progressive failure of the fibers. From these observations, it can be concluded that the polyester specimens have a more ductile-like failure mechanism (i.e., they have more tensile fiber failures and less severe shear failures) than do vinyl ester specimens.

CHAPTER 6. DESIGN CONSIDERATIONS

Data Analysis, Testing, and Design

Several data analysis techniques have been presented here and the question arises, how can these analysis techniques be applied to the design of dynamically loaded structures composed of composite materials? An exact methodology for applying test data of small coupon samples to the design large full-size structures is often complex or impossible to formulate. However, in a general sense, the results of experimental data, such as the results presented here, can be utilized to provide pertinent information regarding material behavior. This can be directly applied to the testing of material and the design of structures. One data analysis technique that yields information about a material is the standard deviation plot technique used in this investigation. The standard deviation of load versus time data for each specimen type is plotted plus and minus the average curve producing a band-like plot. This plot is useful for a number of reasons. It can easily show the relative scatter of data in a neat and legible fashion as opposed to the cluttered multiple curve plots used in many studies. Another way this plot is useful is to predict the load values of test data. From the standard deviation, there is a high probability that specimens tested will produce load versus time plots that fall within the banded region. Also, as a design consideration, using the lower boundary of the plot (average minus one standard deviation) may provide insight into load values to be used for design. In this way, full use can be made of the energy-absorbing characteristics that occur between the initiation energy and the energy at the maximum load.

Future Investigations

Before a full-scale prototype barrier can be developed, additional investigations on the impact response of these materials are necessary. Considering the results presented here, it is logical to proceed on a larger scale using a polyester resin and combinations of fiber orientations. The full potential of the angle-ply material has not been determined through the testing method used (i.e., the specimens did not fail). Therefore, the development of methods to test the angle-ply would be useful in determining if this fiber geometry would enhance a rail structure's properties if included in the lay-up. The testing of structural shapes to optimize desirable shape characteristics would also be useful. This can be performed on a one-third scale in a laboratory environment in an impact test machine, such as the one used in this study. A comparison of existing, currently used guardrail material may also be informative at this stage. Once fiber orientation and shape are optimized, the development of a full-scale prototype can begin. It is conceivable that a composite rail could, at least initially, be used in conjunction with available post systems used on guardrails. However, because of the vast differences between the behavior of steel and composites, a new post system designed to optimize the characteristics of the composite rail needs to be developed.



CHAPTER 7. CONCLUSIONS

The purpose of this study has been to gain an understanding of the impact characteristics of glass fiber-reinforced materials in order to determine their suitability for roadside safety barrier applications. In summary, the following knowledge has been gained on the behavior of composite materials. First, for a guardrail composed of composite materials, longitudinal fibers along the length of the barrier are needed to prevent the impacting car from penetrating through the barrier and to dissipate energy from the collision. Second, fibers oriented along some other directions [e.g., ± 0.785 rad (45°)] may provide additional deflection characteristics desirable for a guardrail structure. Third, polyester resin composites seem to possess more ductile-like impact failure modes (i.e., non-catastrophic failures) than do vinyl ester composites. This non-catastrophic type of failure mode is more suitable for requirements of a guardrail than the catastrophic, abrupt failure found in vinyl ester composites. Fourth, averaging data at every point in time along a curve provides an adequate representation of the behavior of several of one type of test specimen. Using the average curve for data analysis is often simpler than individual data curves because averaging, to some extent, removes the oscillations produced by dynamic test data. This results in a smoother curve that is easier to read. And fifth, normalization by all geometric parameters present in the test allows for the comparison of test data from a variety of material types and test geometric conditions.

In general, glass fiber-composite materials show promise for use in roadside safety barrier applications. However, further testing of these materials, including testing on a larger scale is necessary before a full-scale prototype guardrail can be developed.

REFERENCES

1. Svenson, A. L., Hargrave, M. W., and Bank, L. C., (1993), "Impact Behavior of Pultruded Composites," *Proceedings of the SPI Composites Institute 48th Annual Conference and Exposition*, Cincinnati, Ohio, February 8-11, 1993, Session 21-D, pp. 1-6.
2. Michie, J. D., (1981), *NCHRP Report 230, Recommended Procedures for the Safety Performance Evaluation of Highway Appurtenances*, Transportation Research Board, Washington, DC.
3. Svenson, A. L., Hargrave, M. W., and Bank, L. C., (1992), "Impact Performance of Glass Fiber Composite Materials for Roadside Safety Structures," *Advanced Composite Materials in Bridges and Structures, First Conference*, Sherbrooke, Quebec, Canada, October 7-9, 1992, pp. 559-568.
4. Adams, D. F., (1977), "Impact Response of Polymer-Matrix Composite Materials," *Composite Materials: Testing and Design (Fourth Conference)*, ASTM STP 617, American Society for Testing and Materials, pp. 409-426.
5. Ireland, D. R., (1974), "Procedures and Problems Associated with Reliable Control of the Instrumented Impact Test," *Instrumented Impact Testing*, ASTM STP 563, American Society for Testing and Materials, pp. 3-29.
6. Wardle, M. W. and Zahr, G. E., (1987), "Instrumented Impact Testing of Aramid-Reinforced Composite Materials," *Instrumented Impact Testing of Plastics and Composite Materials*, ASTM STP 936, American Society for Testing and Materials, pp. 219-235.
7. Agarwal, B. D. and Broutman, L. J., (1990), *Analysis and Performance of Fiber Composites*, Second Edition, John Wiley and Sons, New York, pp. 314-339.
8. Gause, L. W. and Buckley, L. J., (1987), "Impact Characterization of New Composite Materials," *Instrumented Impact Testing of Plastics and Composite Materials*, ASTM STP 936, American Society for Testing and Materials, pp. 248-261.
9. Roche J. L., and Kakarala, S. N., (1987), "Methodology for Selecting Impact Tests of Composite Materials in Automotive Applications," *Instrumented Impact Testing of Plastics and Composite Materials*, ASTM STP 936, American Society for Testing and Materials, pp. 24-43.
10. Ross, T., "Vacuum Bagging: A Versatile Processing Tool," *Reinforced Plastics*, May 1992, pp. 22-23.

